Black phosphorus photonics toward on-chip applications (F)

Li Huang (iD), and Kah-Wee Ang (iD)

COLLECTIONS

(F) This paper was selected as Featured

View Online   Export Citation   CrossMark

AVS Quantum Science

SUBMIT TODAY!

SPECIAL ISSUE:
Quantum Sensing and Metrology

Co-Published by
AIP Publishing   AVS

Black phosphorus photonics toward on-chip applications Ⓕ

View Online   Export Citation   CrossMark

Li Huang ⓘD and Kah-Wee Ang[a] ⓘD

AFFILIATIONS

Department of Electrical and Computer Engineering, National University of Singapore, 4 Engineering Drive 3, 117583, Singapore

[a]Author to whom correspondence should be addressed: eleakw@nus.edu.sg

ABSTRACT

Unceasing efforts have been devoted to photonics based on black phosphorus ever since it came under the spotlight of two-dimensional materials research six years ago. The direct bandgap of black phosphorus is tunable by layer number, vertical electric field, and chemical doping, covering a broad spectrum for efficient light manipulation. The optical anisotropy further enables the identification and control of light polarization. Along with high carrier mobility, nonlinear optical properties, and integration capability due to its layered lattice structure, black phosphorus manifests itself as a promising multipurpose material for chip-scale optoelectronics. In this manuscript, we review the research on black phosphorus photonics, with a focus on the most fundamental active functions in photonic circuits: photodetection, electro-optic modulation, light emission, and laser pulse generation, aiming at evaluating the feasibility of integrating these black phosphorus-based components as a compact system for on-chip applications.

TABLE OF CONTENTS

I. INTRODUCTION

The past few years have witnessed a burgeoning research interest in black phosphorus (BP) and its applications in photonics.[1–3] BP is an allotrope of the element phosphorus with a layered lattice structure and a valuable member of the two-dimensional materials family. Yet, BP distinguishes itself from the other two-dimensional materials due to its unique properties.[1,4–6] Within a single layer, each phosphorus atom is connected to three nearest neighbors via covalent bonds.[6] The covalent bonds are along the orbitals formed by sp^3 hybridization, constructing an orthorhombic crystal lattice with a puckered honeycomb structure.[7] Layers are vertically stacked by van der Waals force. The surface of the BP thin film is free from dangling bonds, eliminating the issue of lattice mismatch and making BP compatible with a variety of substrates, including Si, sapphire, and transparent/flexible polymers. The high carrier mobility within the BP layer plane[8–10] allows the realization of optoelectronic devices with high performance. The bandgap of BP is dependent on the layer number and ranges from 0.3 eV for films thicker than 4 nm to 2 eV for a monolayer.[6,11] The energy band of BP bridges the gap between graphene with zero bandgap and transition metal dichalcogenides (TMDCs) with a relatively larger bandgap and covers a wide electromagnetic spectrum, including the mid-infrared, which is beyond the limit of Si and Ge.[6,12] More importantly, the bandgap is always direct regardless of the thickness of BP,[13] making it a favorable material for efficient photodetection and light emission. The conduction band minimum and valence band maximum of BP mainly originate from the $3p_z$ orbital, which is perpendicular to the layer plane.[14] As a result, the bandgap is sensitive to a vertical electric field and could be dynamically tuned by an external bias,[15–17] which could be exploited for electro-optic modulation.[18] Besides, the all-optical modulation in BP could be realized using its saturable absorption property.[19] Another extraordinary feature of BP is the anisotropic in-plane lattice structure. The asymmetry of BP's crystal structure leads to anisotropic optical properties, such as refractive index, extinction coefficient, and exciton effects,[11,20–27] which could be utilized to realize photonic devices for the detection and manipulation of light polarization.[27,28]

With these superior features, BP is anticipated to be a versatile material for diversified photonic building blocks, including the most essential ones such as photodetectors, modulators, and lasers. While

the traditional materials for mid-infrared are facing the challenge of integration difficulty,[29–32] BP's narrow and tunable bandgap together with its integration compatibility is especially competitive for chip-scale mid-infrared photonic systems, with which abundant applications[12,33–36] such as bio-molecule screening, autonomous car guiding, and landscape mapping could be envisaged. Here, we review the research on BP photonics, categorizing them into four groups according to BP's function: photodetection, electro-optic modulation, light emission, and laser pulse generation. In the concluding remarks, we will also discuss the outlook and challenges, and propose a pathway for integrating these basic functions into a photonic circuit for practical on-chip applications.
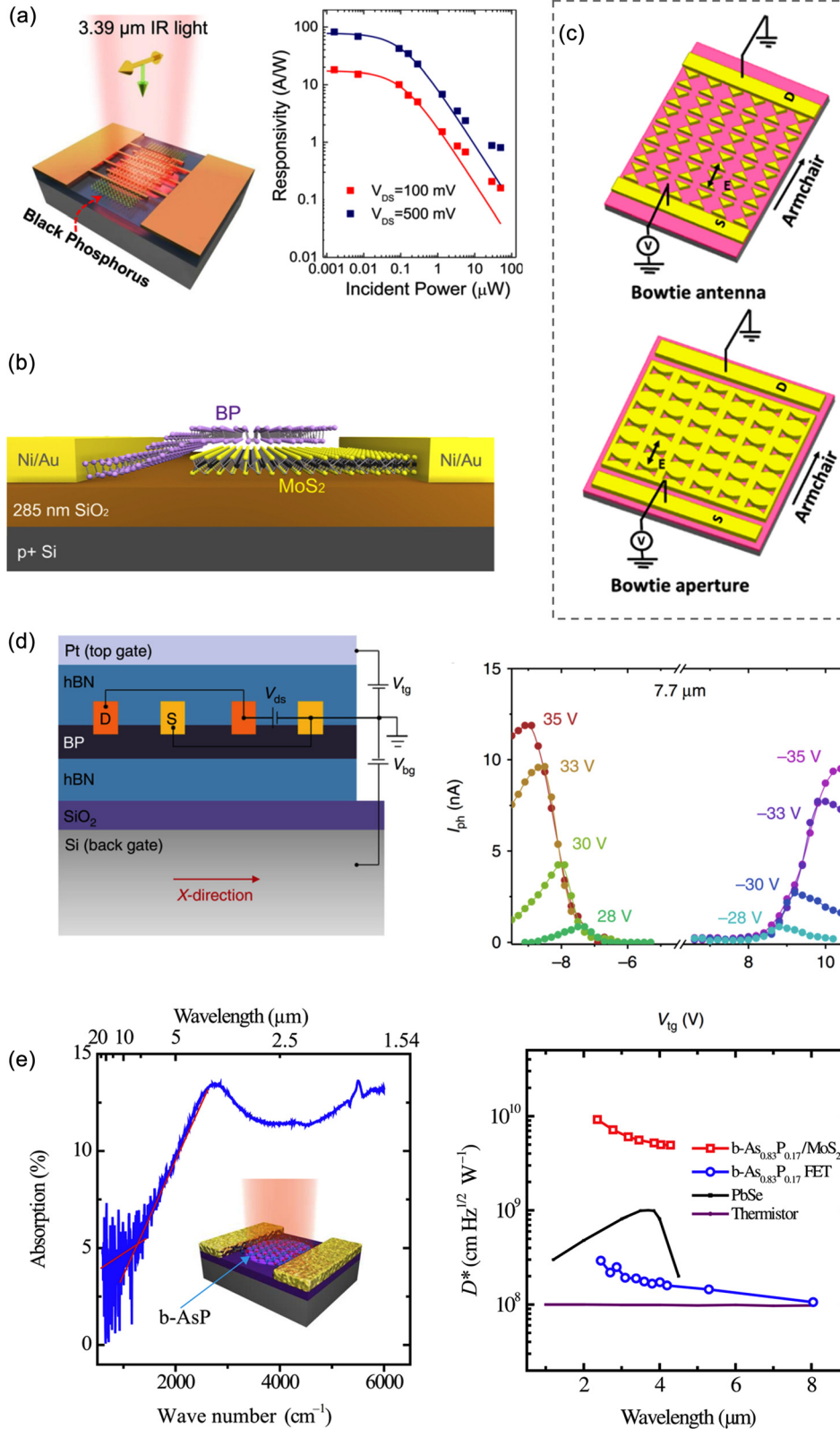
II. BP PHOTODETECTORS

Photodetectors are optoelectronic devices, which serve to convert light signal to electric signal. Applications of photodetectors include imaging, data communication, sensing, and light detection and ranging (LiDAR). Benefits of using BP as the detection material are integration compatibility, high responsivity under weak power, broadband detecting range, including mid-infrared, and polarization sensitivity.

Based on the broadband properties of BP, photodetectors for varying wavelengths from ultraviolet to infrared have been demonstrated.[37–43] The most basic configuration of a photodetector is the detection material with two electrodes for photocurrent collection, as adopted by some of the works on the BP photodetector.[39,43,44] However, the widely explored device structure is the back gate BP transistor on the SiO$_2$/Si substrate [Fig. 1(a)].[37,38,40–42,45,46] With a gate bias to tune the carrier concentration in the BP channel, the transistor could be turned off with a low dark current, which is an advantage of BP's moderate bandgap over graphene's zero bandgap. The gate bias impacts not only on the dark current but also on the photocurrent. The trap-induced photoconductive gain, contact barrier height, photogating effects, and even the BP's bandgap are all subject to gate bias, which would further affect the photocurrent generation and detection speed.[40,41,45,47–49] However, in some cases, the detectors had to be operated at the on-state of the transistor to achieve high responsivity at the cost of a high dark current, because the gate bias needed to achieve low barrier height for photocarriers coincided with the on-state bias.[37,45] To avoid such trade-off and make full use of the advantage offered by BP's bandgap, the pristine doping condition and the thickness of BP together with the contact material with a suitable work function need to be preselected with considerate design such that the photocurrent could be enhanced while dark current could be simultaneously suppressed.

Forming p–n junctions and operating the detector with a reverse or zero bias are other methods to suppress the dark current. In addition, the junction area with a built-in electric field helps to separate and collect photogenerated carrier pairs more efficiently. Photodetectors based on BP homojunctions formed by electrostatic gating,[50,51] chemical doping from the capping layer,[52,53] and different BP thicknesses,[54] as well as heterojunctions formed by BP with an n-type two-dimensional material [Fig. 1(b)][55–58] or phosphorene oxide,[59] have been reported. Constructing heterojunctions using an n-type material and BP has also been explored to initiate impact ionization in BP with a low avalanche threshold. Ballistic avalanche phenomena in a vertical InSe/BP heterostructure have been observed, which were utilized to demonstrate an avalanche photodetector with a multiplication

of 10^4 at a wavelength of 4 μm under a temperature of 10 K.[60] However, their device was functional only at cryogenic conditions, because the avalanche breakdown started to be replaced by the Zener breakdown when the temperature was increased to 200 K. While low-temperature measurement is useful in the study of material physics, practical applications favor room-temperature operations with high thermal stability.

Polarization sensitivity is an additional advantage of BP as a result of its anisotropic in-plane lattice structure. This has been verified through polarization-dependent transmission spectra and photocurrent in BP.[37,40,61] Polarization carries more information of light, such as the history of light–matter interaction.[62] Detection of not only the intensity but also the polarization of light could be utilized for many applications, such as enhancing the visibility of automobile in hazy and rainy weather,[62] differentiating natural objects from man-made materials,[63] and identifying the three-dimensional orientation of bio-molecules.[64] While almost every BP photodetector showed polarization sensitivity as a result of the inherent anisotropic absorption in BP, most of them failed to resolve the polarization of light because they could not decouple the effects from the intensity and polarization of the light source. To improve the polarization sensitivity in BP, a few device structures have been proposed. Forming a vertical homogeneous p–n junction is one of the methods to enhance linear dichroism photodetection.[51] The results showed that by applying a perpendicular electric field, responsivity for armchair polarization could be increased. Plasmonic resonance in the periodic metal structure [Fig. 1(c)] has also been explored to enhance polarization sensitivity.[65] Nevertheless, the enhancement is not effective enough, possibly due to a lack of optimization. It is worth noting that introducing metal nanostructures into devices for infrared also comes with the risk of bringing in extra loss. The polarization dependence in these works is only in the level of a few times and is not strong enough to identify the polarization of light source. In an effort to strengthen the polarization sensitivity to such a level that polarization could be truly discerned regardless of the light intensity, photodetectors based on BP (armchair)/MoS$_2$/BP (zigzag) heterojunctions have been proposed to achieve polarization-selectivity.[27] The crystal orientation of BP in the two BP/MoS$_2$ junctions is orthogonal, and active junction in their photodetector is bias-selectable. This device configuration is capable of breaking down the polarization of light along two orthogonal directions. Although the device being demonstrated is only capable of narrowing down the polarization to two directions, this design concept could be implemented to realize polarization detectors by stacking one more polarization-selective heterostructure of BP (armchair)/MoS$_2$/BP (zigzag) with a different crystal orientation alignment from the previous one. In addition, the refractive index and extinction coefficient in mid-infrared were extracted from the reflection spectra of the samples, for both armchair and zigzag orientations of BP. The anisotropic dielectric permittivity and the optical conductivity for shorter wavelengths have been reported in previous studies,[20,26] which could be used to extract complex refractive indexes. Among the armchair, zigzag, and out-of-plane directions, both the real and imaginary parts of the refractive index in BP are larger along the armchair orientation and are smallest for the out-of-plane direction. The anisotropic refractive index and extinction coefficient are crucial parameters for designing the photonic devices based on BP, as they determine the light distribution and propagation, as well as light–BP interaction.

FIG. 1. Surface-illuminated BP photodetectors. The light from free space interacts with BP transiently due to the small BP thickness. (a) Mid-infrared BP photodetector and its power-dependent responsivity at 3.39 μm. Higher responsivity under lower power is caused by the saturable trap-induced photoconductive gain. A transistor with a back gate is the most widely explored structure for BP photodetectors. The dark current, photoconductive gain, contact barrier height, and photogating effect are all subject to gate bias, further impacting on the responsivity and speed of the photodetector. Reproduced with permission from Guo *et al.*, Nano Lett. **16**(7), 4648–4655 (2016). Copyright 2016 American Chemical Society.[40] (b) BP/MoS$_2$ heterojunction for photodetection. A vertical junction with a large active area improves photocarrier collection efficiency. A p–n junction also enables operation with zero bias. Reproduced with permission from Deng *et al.*, ACS Nano **8**(8), 8292–8299 (2014). Copyright 2014 American Chemical Society.[55] (c) BP photodetectors with a plasmonic structure for enhancing light absorption and polarization sensitivity. Plasmonic effect could confine light from free space into a localized space for stronger light–matter interaction, which is usually polarization sensitive. However, metal nanostructures could also introduce a huge loss in mid-infrared. Reproduced with permission from Venuthurumilli *et al.*, ACS Nano **12**(5), 4861–4867 (2018). Copyright 2018 American Chemical Society.[65] (d) Photodetection up to 7.7 μm enabled by applying a vertical electric field in BP. Reproduced with permission from Chen *et al.*, Nat. Commun. **8**(1), 1672 (2017). Copyright 2017 Springer Nature.[48] (e) Absorption of BP extended to 10 μm by arsenic doping (left) and the detectivity of a b-As$_{0.83}$P$_{0.17}$ photodetector of up to 8 μm (right). Reproduced with permission from Long *et al.*, Sci. Adv. **3**(6), e1700589 (2017). Copyright 2017 American Association for the Advancement of Science.[58] Between the two approaches to extending the BP's detection wavelength, electrostatic tuning is reversible and dynamic, while chemical doping is permanent and does not require an extra source of power in operation.

Although BP shows great potential in the mid-infrared, the detection spectrum of BP is still limited by its bandgap. The absorption is cut off at the wavelength of ~4.1 μm for the BP thin film thicker than 4 nm.[6] For thinner BP, the cut-off wavelength would be even shorter as the bandgap broadens. Two approaches have been explored to extend the detection range of BP to longer wavelengths. The first approach is to apply a vertical electric field to tune the bandgap of BP through the Stark effect.[15,17] This method has been exploited to realize the photodetection of up to 7.7 μm under a cryogenic condition of 77 K [Fig. 1(d)].[48] The second approach is to dope BP with arsenic atoms to form black arsenic-phosphorus (b-AsP). Introducing As could further shrink the bandgap, which monotonously narrows with higher As concentration.[66,67] Room-temperature photodetection of up to 8.05 μm has been demonstrated with b-AsP as the detection material [Fig. 1(e)].[58,68] By extending the detection spectrum beyond 4 μm, many more sensing applications could be realized as many molecules show characteristic absorption in the 4–8 μm spectral range.[69] Besides using As, doping BP with potassium,[70] selenium,[71] and carbon[72,73] has also been explored to reduce BP's bandgap. The electrostatic tuning is reversible and dynamic, while the chemical doping method is permanent and may introduce impurity scattering in the BP channel.

While most of the published works on BP photonics are stand-alone devices, integrated photodetectors start to attract growing attention from the research community. Integration with waveguides does not only come with the advantage of enhanced light–BP interaction but also opens the door for realizing advanced functions such as on-chip sensing, which requires an integration of different optoelectronic components in a compact system. BP photodetectors integrated with the Si waveguide were first reported at a wavelength of 1550 nm, and the active part is a BP transistor with a graphene top gate.[49] However, the responsivity and speed in this work are not competitive enough compared to waveguide photodetectors based on traditional materials[74] for the 1550 nm, a wavelength that has been extensively explored. To improve the responsivity, electrodes with a metal plasmonic nanogap were proposed to enhance light absorption and photoconductive gain in the BP channel [Fig. 2(a)].[75] Although the internal responsivity was increased, the plasmonic nanostructure also introduced huge insertion loss. Besides the metal plasmonic structure, the Si photonic crystal has also been integrated with BP [Fig. 2(b)].[76] Surface illumination was used to map the light scattering in the Si photonic crystal by measuring the photocurrent in BP for the 620–760 nm visible spectrum. Such an integration scheme could be employed for wavelength-selective photodetectors.[77] In the recent two years, more efforts have been dedicated to realizing waveguide-integrated BP photodetectors for longer wavelengths in the short-wave infrared and mid-infrared spectra. BP photodetectors hybridized with Si waveguides were demonstrated at a data receiving rate of 4 Gbit/s at a wavelength of 2 μm [Fig. 2(c)].[78] Besides, BP photodetectors integrated with the chalcogenide glass waveguide were demonstrated for 2–2.5 μm.[79] The chalcogenide glass waveguides were directly deposited on BP and, meanwhile, are compatible with flexible substrates. This work indicates BP's compatibility with a different material platform other than Si, allowing for more diversified integrations. Targeted at the mid-infrared applications, such as label-free and damage-free sensing, waveguide-integrated photodetectors for wavelength beyond 3 μm were demonstrated [Fig. 2(d)].[47,80] Devices with different BP crystal orientations and thicknesses were compared in terms of their

responsivity and noise level for the 3.64–4.03 μm. The comparison showed that in optical integrations, the alignment of BP's crystal orientation with the other optical structures had huge impact on the device performance. Under room temperature, the photodetector achieved a high responsivity and a low noise equivalent power, manifesting BP's potential for on-chip mid-infrared applications, such as gas detection and bio-sensing.

III. ELECTRO-OPTIC MODULATION IN BP

The function of an optical modulator is to tune the parameters (such as intensity, phase, frequency, and polarization) of the light signal; thereby, it attaches additional information to the light passing through and then transmits the light for subsequent processes. Modulators could be employed for numerous applications, such as computing and data communication,[81] increasing signal-to-noise ratio for sensing,[82] and steering light beam for light detection and ranging.[83] The optical properties of BP could be modulated by either an electrical signal (electro-optic modulation) or an optical signal (all-optical modulation). The all-optical modulation in BP based on saturable absorption will be discussed in Sec. V. So far, the reported works on the electro-optic modulation in BP are mainly based on the change of absorption.

Theoretical calculations have shed light on BP's tunable bandgap under a vertical external field [Fig. 3(a)].[14,84] The anisotropic optical properties in the thin film BP were investigated at a temperature of 300 K.[20] The optical conductivity along the armchair direction is higher than that of the zigzag direction. Oscillatory behavior originated from sub-band structures is presented in the spectral optical conductivity for the armchair orientation but is absent for the zigzag orientation. The absorption edge moves to higher energy as BP's thickness increases. With the thickness increased by 1 nm, the absorption increases by 0.4%. Their results show that the spectral optical conductivity is also sensitive to the doping condition in BP. With increasing doping concentration, the absorption edge exhibits a blue shift due to Pauli blocking [Fig. 3(b)], which is the underlying mechanism for the Burstein–Moss (BM) effect. Besides, the absorption edge also becomes less abrupt at higher doping. The calculation results reveal that the light absorption in BP could be modulated by an external electric field through Fermi level tuning, which could be exploited to realize electro-optic modulators.

To assess BP's potential performance as an active material for modulator, sub-band transitions in BP were theoretically examined, and the gate modulation of the optical loss in a BP/Si waveguide structure was calculated [Fig. 3(c)].[85] The shift of BP's absorption edge by an electric field was caused by a combination of the quantum confined Franz–Keldysh (QCFK) effect and the Burstein–Moss (BM) effect. The optical conductivity and bandgap shift were quantitatively analyzed as a function of the carrier concentration and photon energy for BP thin films with different thicknesses. The calculations indicate that the QCFK effect is dominant at low carrier concentration, while the BM effect is dominant at high carrier concentration. Based on the calculations, a model of BP on the Si waveguide was studied as a modulator. The waveguide loss changes more abruptly with gate bias under the QCFK scheme, which directly changes the energy bandgap. In the BM effect, the waveguide loss changes gradually with gate bias due to thermalization of electrons, where the absorption edge becomes less sharp. The calculations show that as a material for mid-infrared
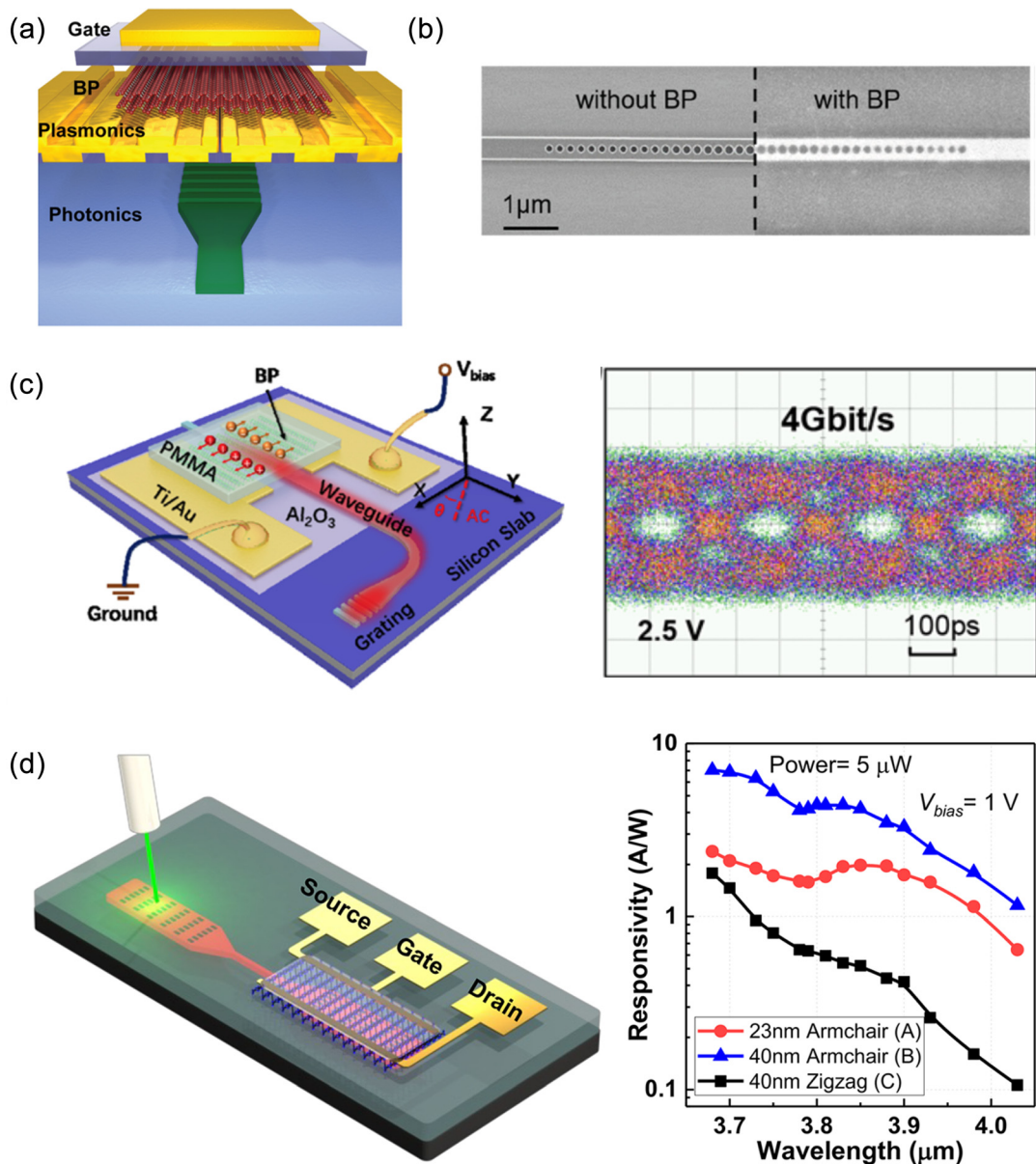
FIG. 2. Waveguide-integrated BP photodetectors. Waveguide integration does not only enhance light–BP interaction but also opens up avenues for connecting with other photonic components. (a) BP photodetector integrated with waveguide and metal plasmonics at 1.55 μm. The plasmonic nanogap enhances light absorption and photocarrier collection. However, the metal nanostructure also introduces extra loss in the waveguide. Reproduced with permission from Chen *et al.*, Nano Lett. **17**(2), 985–991 (2017). Copyright 2017 American Chemical Society.[75] (b) BP on top of the Si photonic crystal waveguide for visible light. The BP photodetector was implemented to visualize light scattering in the Si photonic crystal. Such an integration could also be adopted for wavelength selective detection. Reproduced with permission from Wang *et al.*, Adv. Mater. **28**(33), 7162–7166 (2016). Copyright 2016 WILEY-VCH.[76] (c) BP photodetector integrated with the Si waveguide at a 2 μm short-wave infrared (left) and the eye diagram at a 4 Gbit/s data rate. Reproduced with permission from Yin *et al.*, Laser Photonics Rev. **13**, 1900032 (2019). Copyright 2019 WILEY-VCH.[78] (d) Mid-infrared waveguide-integrated BP photodetector and the spectral responsivity of devices with different crystal orientations and thicknesses. With the strongly anisotropic properties, the alignment of BP's crystal orientation will play a crucial role in optimizing device performance for photonic integration. Reproduced with permission from Huang *et al.*, ACS Nano **13**(1), 913–921 (2019). Copyright 2019 American Chemical Society.[47]

electro-optic modulation, BP could achieve better performance than graphene in terms of extinction ratio and power consumption.

The theoretical predictions have also been verified by experimental results. By analyzing the carrier transport properties in a dual-gate BP transistor, the bandgap tuning in the thin film BP by a vertical electric field was investigated [Fig. 3(d)].[15] The bandgap of BP was experimentally extracted from the minimum conductance of the transistor under varying vertical electric field and different temperature. Their
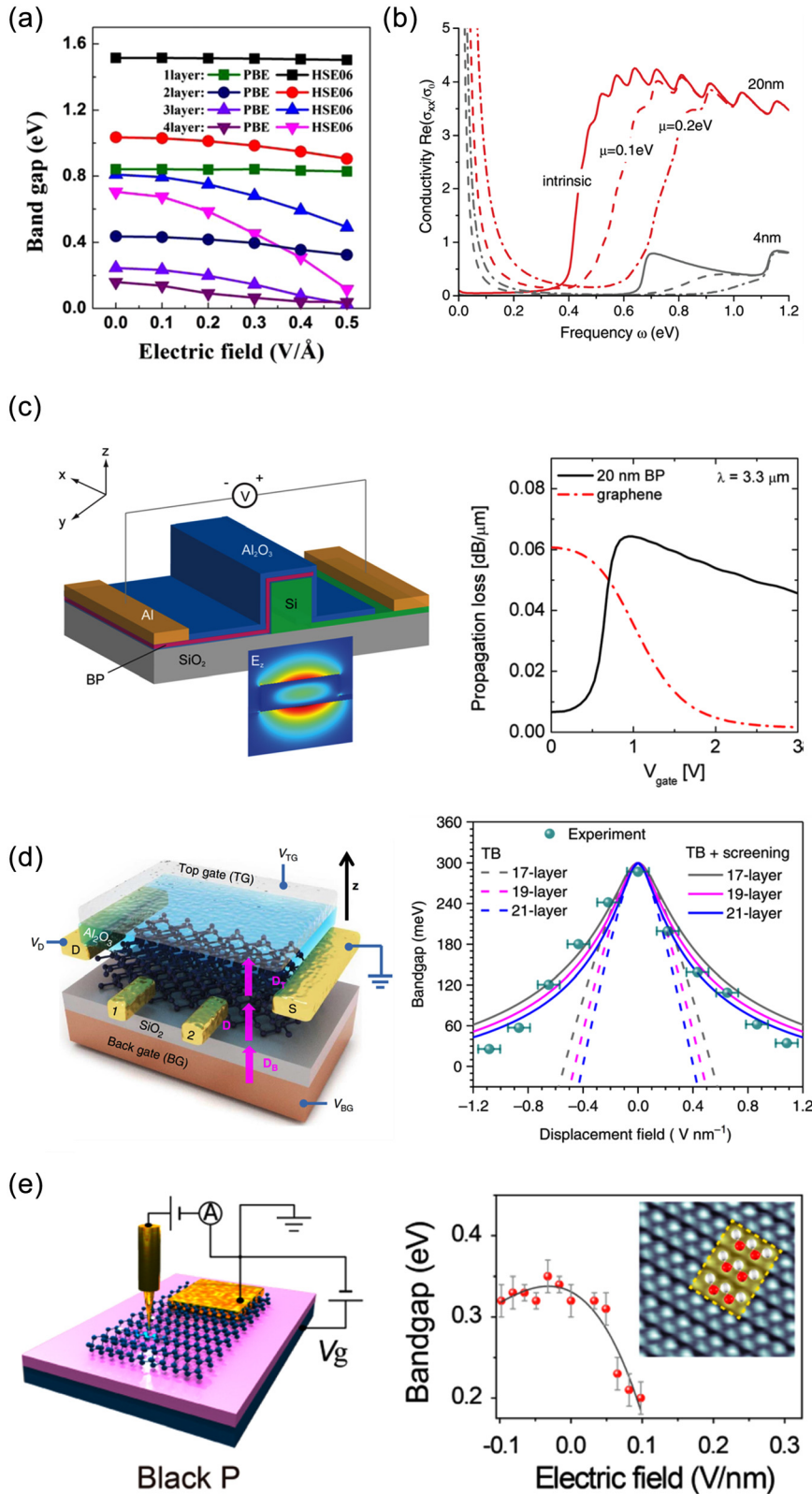
FIG. 3. Theoretical predictions (a–c) of the electro-optical modulation in BP and its verification by bandgap measurement (d, e). (a) Bandgap tuning in BP by a vertical electric field by calculated density functional theory. The tuning effect is more significant with a larger layer number as a result of the interlayer interaction. Reproduced with permission from Guo et al., Phys. Chem. C **118**(25), 14051–14059 (2014). Copyright 2014 American Chemical Society.[84] (b) Numerical calculation of the absorption edge shift in BP under different doping conditions due to Pauli blocking. The optical conductivity is highly anisotropic (the armchair properties are presented here). Reproduced with permission from Low et al., Phys. Rev. B **90**(7), 075434 (2014). Copyright 2014 American Physical Society.[20] (c) Calculation of the gate-tuned propagation loss in a BP on the Si waveguide design model. Compared to graphene, BP could achieve a higher extinction ratio with a smaller gate bias, indicating a larger modulation depth and a lower power consumption for modulator applications. Reproduced with permission from Lin et al., Nano Lett. **16**(3), 1683–1689 (2016). Copyright 2016 American Chemical Society.[85] (d) Measured bandgap in a dual-gate BP transistor, showing the effective bandgap tuning by a vertical electric field. Stronger modulation presents in thicker BP due to a larger Stark coefficient. However, the optimal thickness could be 10–15 nm, considering the screening effect. Reproduced with permission from Li et al., Adv. Mater. **30**(6), 1703748 (2018). Copyright 2017 Springer Nature.[15] (e) Stark effect in BP measured by low-temperature scanning tunneling microscopy. An effective bandgap reduction by more than one third is obtained with an electric field as low as 0.1 V/nm. A low voltage requirement would be favorable for CMOS integration. Reproduced with permission from Liu et al., Nano Lett. **17**(3), 1970–1977 (2017). Copyright 2017 American Chemical Society.[17]

results show that the bandgap of a 10 nm-thick BP flake could be effectively reduced from 0.3 eV to 0.05 eV by applying a vertical displacement field of 1.1 V/nm. Such a voltage requirement could be easily achieved in integrated circuits with a thin gate dielectric layer of high quality. The tuning effect is weak in BP films thinner than 4 nm, as a result of the smaller Stark coefficient for BP with smaller thickness. However, a large thickness (>23 nm) could also compromise the bandgap tuning efficiency due to the dielectric screening effect. Therefore, the authors suggested that for optoelectronic applications, the optimal thickness of BP might be 10–15 nm.

Bandgap tuning in BP was also observed in low-temperature scanning tunneling microscopy, through the gate-induced Stark effect in which the band structure shifts and splits due to wavefunction redistribution under the external electric field.[17] Experimental results and the calculation by density functional theory showed that both the valence band and the conduction band shift to lower energy under positive bias, but with the conduction band shifting down more than the valence band, resulting in the shrinking of bandgap. A bandgap reduction of 35.5% was achieved by applying a gate bias of 0.1 V/nm in an 11-layer BP flake [Fig. 3(e)], verifying the effectiveness of gate tuning.

These results indicate that efficient bandgap tuning could be achieved with a small voltage bias, making BP a promising material for broadband optoelectronics. In addition to the measurements of electrical behavior, the band structure tuning by a vertical electric field has also been manifested through measuring the optical properties of BP. The field-effect modulation of the BP's optical properties was experimentally verified via measuring the transmission spectra of BP on the SiO_2/Si substrate at a temperature of 80 K with an elliptically polarized light source [Fig. 4(a)].[86] BP flakes with different thicknesses and doping conditions were measured and analyzed with the theoretical calculation of the optical conductivity. The applied electric field could lead to either red or blue shift of the absorption edge, depending on the thickness and initial doping of the BP flakes. Based on a similar sample structure, the electro-optic modulation in BP focusing on the mid-infrared spectrum was investigated using a linearly polarized light source at room temperature [Fig. 4(b)].[87] The modulation of light polarized along the zigzag orientation of BP was much weaker than that for the armchair orientation. The polarity of the modulation in their sample was dependent on the photon energy and the polarity of gate bias. The sign of the transmission modulation was attributed to both band shifting and the change of wavefunction overlap.

The modulation amplitude in the previous two works is only around 2%, due to the limited transient light–BP interaction in surface-illuminated structures. Through waveguide integration, a small amount of change in the extinction coefficient could be converted to a large modulation depth, as demonstrated by a Si-waveguide-integrated BP modulator for mid-infrared.[88] The modulation depth was observed to be increasing with decreasing light power and reached −5 dB with a small gate bias of −4 V, with a trend to be even larger if the power of light could be further decreased. The footprint and the power consumption of the BP modulator are also significantly smaller and lower than the mid-infrared modulators based on conventional materials.

In order to differentiate the modulation mechanisms and separate them in the measurements, a sample structure with dual-gates was adopted [Fig. 4(c)] and the anisotropic electro-optic modulation in BP was investigated for spectral range from visible to mid-infrared.[28]

Three competing modulation mechanisms were used to interpret the observations: the Burstein–Moss effect, the quantum confined Stark effect, and the modification of quantum well selection rule due to symmetry breaking. To distinguish these effects in the transmission measurements, BP samples were measured under different bias schemes. With bias applied through the two gates and BP being floating, the carrier concentration in BP remained unchanged so that the BM effect was eliminated. With external field applied through the bottom gate while BP contacted, where the carrier concentration effects were allowed, the BM effect was dominant. The modulation of transmission was observed for light polarized along the armchair axis of BP, while being absent for zigzag polarization. The anisotropic modulation indicates that the linear dichroism and birefringence could be electrically controlled, and the absorption of BP could be tuned from anisotropic to isotropic, offering avenues to control light polarization, phase, intensity, and propagation.

IV. LIGHT EMISSION IN BP

Besides photodetector and optical modulator, photonic circuits would not be complete without light emitting devices, which serve as the source of the optical signal. As a direct bandgap material, BP holds great potential for efficient light emission.

The investigation of BP's light emitting properties started with the characterization of photoluminescence. Layer-dependent (2–5 layers) photoluminescence in BP was observed, with the emission peak red shifting as the layer number was increased [Fig. 5(a)], due to the interlayer interaction, which reduces the bandgap.[89] The peak intensity decreased with an increase in the layer number. The lower internal luminescence quantum efficiency in BP with more layers was ascribed to the band structure changed by the layer number. It is claimed that more valleys and maxima in the band structure of a 5-layer BP caused higher electron relaxation rate than a 2-layer BP. Besides, the photoluminescence of a few-layer BP was much stronger than that of the bulk Si substrate, revealing that the advantage of having a direct bandgap overcomes the weakness of being atomically thin.

To achieve light emission with different visible wavelengths in the same sample, laser oxidation has been explored to thin down BP flakes and form phosphorene oxide thin films.[90] The bandgap and thickness of the phosphorene oxide could be adjusted by laser power. The phosphorene oxide was observed to emit light in the visible spectral range under ultraviolet and visible excitations [Fig. 5(b)]. The laser oxidation process had introduced defect levels in the band structure, enabling light emission with multiple colors under different excitation wavelengths. The phosphorene oxide could be reduced to phosphorus when being exposed to ammonia (NH_3) gas. After NH_3 exposure, the PL intensity was largely reduced and could be partly recovered by re-oxidization using laser beam. The results imply potential applications such as multicolor displays and toxic gas monitors.

Similar to the light absorption and modulation, which are polarization dependent, the photoluminescence in BP is also anisotropic. Polarization-resolved photoluminescence in BP ranging from visible to near-infrared spectra was observed.[91] Along the armchair polarization, strong photoluminescence was observed with peak wavelength matching the absorption edge of the BP thin film, an indication of the BP's direct bandgap. The photoemission polarized along the zigzag orientation was absent, due to the forbidden optical transition along the zigzag orientation by symmetry requirements.
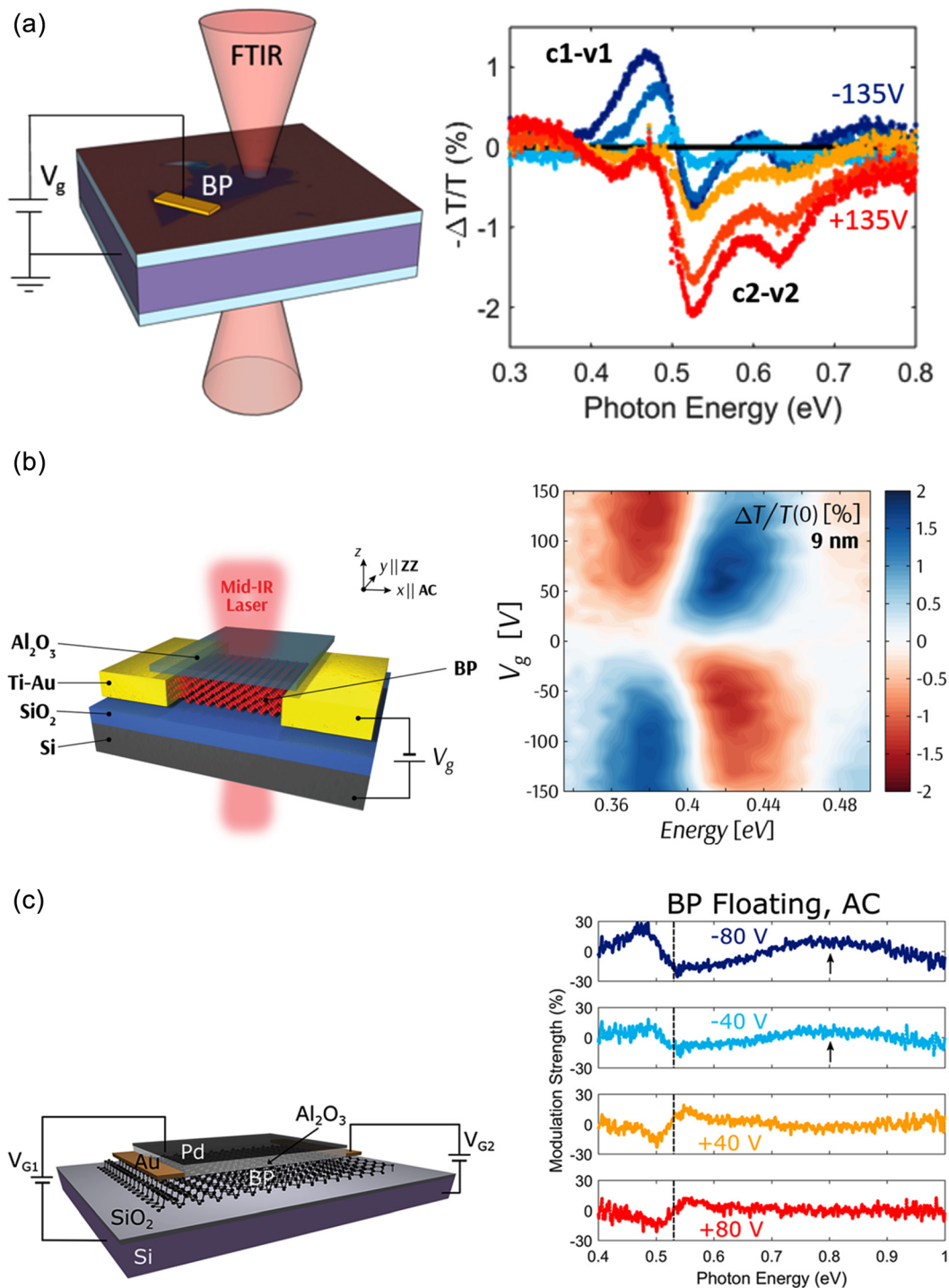
FIG. 4. Gate modulation of the transmission of (a) a heavily p-doped 6.5 nm BP flake at 80 K, (b) a lightly p-doped 9 nm BP flake under room temperature, and (c) a floating 3.5 nm BP flake with quantum confined Franz–Keldysh effect dominant. Two mechanisms account for the electro-optical modulation: the shift of energy bands and band filling tuned by the vertical electric field. The dominant mechanism is dependent on the thickness and initial doping of BP and could also be controlled by connecting BP to ground or leaving it floating. The characteristic wavelengths in the spectra result from the sub-band transitions in BP. Light polarized along the armchair orientation could be effectively modulated, while light with the zigzag polarization presents negligible modulation. Reproduced with permission from (a) Whitney *et al.*, Nano Lett. **17**(1), 78–84 (2017). Copyright 2017 American Chemical Society.[86] (b) Peng *et al.*, Nano Lett. **17**(10), 6315–6320 (2017). Copyright 2017 American Chemical Society.[87] (c) Sherrott *et al.*, Nano Lett. **19**(1), 269–276 (2019). Copyright 2019 American Chemical Society.[28]
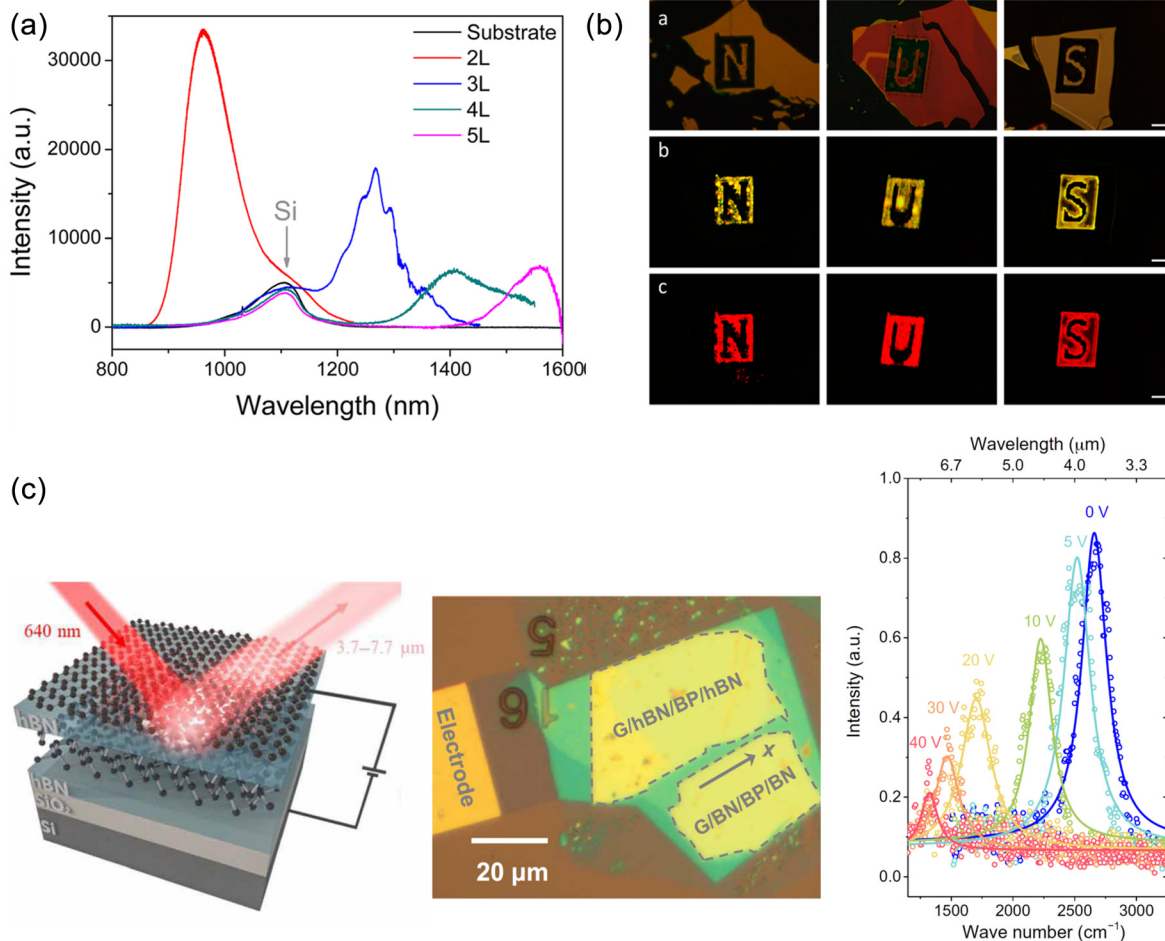
FIG. 5. Photoluminescence in BP ranging from visible to mid-infrared. (a) Layer-dependent photoluminescence. Emission wavelength shows a red shift for a larger layer number due to interlayer coupling. The photoluminescence from BP presents a higher intensity than that from the Si substrate, manifesting the advantage of direct bandgap. Reproduced with permission from Zhang *et al.*, ACS Nano **8**(9), 9590–9596 (2014). Copyright 2014 American Chemical Society.[89] (b) Multicolor emission in laser-modified BP (phosphorene oxide) under different excitation wavelengths. The defect levels introduced by the laser enable electron transitions with varying energy gap. The phosphorene oxide could be reduced to phosphorus by ammonia gas. Potential applications of such device include multicolor displays and toxic gas monitors. Reproduced with permission from Lu *et al.*, ACS Nano **9**(10), 10411–10421 (2015). Copyright 2015 American Chemical Society.[90] (c) Tunable photoluminescence spectra from 3.7 to 7.7 μm by applying a vertical displacement field of up to 0.48 V/nm. The wide tunable wavelength range allows for extensive potential applications in mid-infrared, such as chemical sensing. Reproduced with permission from Chen *et al.*, Sci. Adv. **6**(7), eaay6134 (2020). Copyright 2020 American Association for the Advancement of Science.[97]

Photoluminescence involved with excitons in the monolayer and few-layer BPs was also observed to be highly anisotropic and presented an optical bandgap smaller than the electrical bandgap by an amount of the exciton binding energy.[11,24,25] The excitonic effect in BP is observable at room temperature, with a strongly layer-dependent binding energy. The binding energy decreases monotonously as the layer number increases, ranging from ∼0.9 eV for monolayer to 0.106 eV for 6-layer, and eventually becomes negligible for BP as thick as ∼30 nm, due to strong interlayer coupling.[2,11,92,93] Besides, the excitons in BP are able to withstand a large in-plane electric field and, thus, can be tuned through the Stark effect.[94] The exciton emission wavelength could be modified by introducing defects in BP with enhanced quantum yield.[95]

Moving to longer wavelengths, mid-infrared photoluminescence from the thin film BP was first reported in a hBN/BP/SiO$_2$/Si sample.[96]

The photoluminescence emission was observed to be linearly polarized along the armchair orientation of BP. The intensity of the photoluminescence emission decreases at higher temperature, due to more nonradiative recombination centers. The position of the main peak in the photoluminescence spectrum exhibited a blueshift with increasing temperature. A side peak insensitive to temperature was speculated to be related to the defects in BP. The blueshift of the main peak was attributed to the bandgap changed by the electron–phonon coupling and lattice thermal expansion under increasing temperature. The photoluminescence intensity of InAs at a wavelength of 2.45 μm was observed to be only a few times higher than that of BP at a wavelength of 4 μm, implying BP's potential in light emitting and even lasing in mid-infrared. Inspired by the previous work of extending the detection wavelength of BP by a vertical electric field, the photoluminescence in

the thin film BP was investigated with a dual-gate for bandgap tuning.[97] The peak position of BP's photoemission could be continuously tuned from 3.7 to 7.7 μm, by applying a vertical displacement field of up to 0.48 V/nm [Fig. 5(c)]. This wide range of wavelengths tuned by the electric field provides extensive opportunities for mid-infrared applications, especially chemical sensing.[69]

While the spontaneous emission is easier to occur, as demonstrated in the aforementioned works, it is more demanding in order to observe the stimulated emission where population inversion of carriers is required. The mid-infrared lasing effect in BP was first demonstrated at room temperature by incorporating BP in a vertical optical cavity constructed with distributed Bragg reflectors (DBRs) [Fig. 6(a)].[98] Instead of being exfoliated from bulk, the BP thin film was grown by the mineral-assisted gas-phase transformation. The layers of the grown BP were not densely squeezed; instead, they formed a lamellar structure of alternating BP layers and nanoscale air gaps. Compared with the BP of densely squeezed layers, the photoluminescence spectrum of the as-grown lamellar BP presented a higher intensity and a narrower full width at half maximum, possibly due to the constructive interference between the nano air gaps. The DBR with high reflectivity for a 3450–3850 nm spectral range consisted of alternating layers of SiO_2/Si_3N_4. At low excitation power, spontaneous emission with a broad spectrum was observed. The onset of stimulated emission occurred when the excitation power was increased to lasing threshold, with a narrower peak rising among the broad spontaneous emission. Under higher excitation power, the stimulated emission spectrum became a sharp peak with a narrow width of a few nanometers. In another work with a similar device structure [Fig. 6(b)], the lasing wavelength was reported to be tunable by the thickness of BP, which serves as the length of the resonant cavity between the top and bottom DBRs.[99] In addition, the lasing polarization from the cavity was observed to be along the zigzag orientation of BP, while the spontaneous photoemission was along the armchair orientation, as a result of the anisotropic round trip loss in the BP cavity. The lasing phenomenon showed good thermal stability with temperature increasing from 296 to 358 K, which is advantageous to the high density integration where considerable heat may be generated during operation.

Most of the works investigated the photoemission in BP using another optical source as the excitation, while the electroluminescence in BP remained unexplored, until recently, mid-infrared light emitting diodes were realized using BP/MoS$_2$ heterojunctions [Fig. 6(c)].[100] The diode consisted of a p-type BP flake and an n-type MoS$_2$ flake formed by the van der Waals stacking on the SiO_2/p-Si substrate, which was also a back gate. With a forward bias applied to the p–n junction, electrons in the conduction band of MoS$_2$ are able to overcome the barrier at the junction formed by the offset between the conduction band minimum of BP and MoS$_2$. The electrons from MoS$_2$ entering the BP's conduction band could further recombine with the holes in BP, emitting photons with energy close to BP's bandgap. With a 7 V forward bias, an electroluminescence spectrum centered at ∼3.6 μm was observed. The intensity of the electroluminescence emission for the armchair polarization was three times that of the zigzag polarization. However, the external quantum efficiency is only 0.03%, partly caused by the unoptimized device layout. The SiO_2/Si substrate has higher refractive index than the air above the device so that the photoemission tends to go downward instead of upward, as verified by the simulated upward coupling efficiency of 3.6%. We could expect the external quantum efficiency to be significantly improved if the geometry of the device could be redesigned to extract the light emission to the desired direction. For example, reflective layers could be introduced to direct the light out-of-plane; meanwhile, grating couplers could be adopted to guide the light for in-plane propagation. On the other hand, the internal quantum efficiency may be enhanced by optimizing the band alignment in the diode junctions. The material and doping condition for each layer should be predesigned so that carriers could be effectively injected into BP and potential barriers could be created for efficient radiative recombination.

V. BP AS A SATURABLE ABSORBER

BP exhibits saturable absorption for a broad spectrum from visible to mid-infrared. Light absorption in BP attenuates under higher light intensity as more electrons get depleted in the valence band. Together with its fast carrier dynamics, BP shows potential as a saturable absorber for ultrafast photonics, such as all-optical modulation and pulsed laser generation with short pulse duration and larger pulse energy.

The nonlinear excitation dynamics in BP was investigated for wavelengths ranging from 800 nm to 2.1 μm.[101] The BP nanosheets were prepared by liquid phase exfoliation and drop cast on to a SiO_2/Si substrate. The pump–probe method was used to measure the transient absorption in BP under different wavelengths and pulse energy. Compared with graphene, BP showed faster carrier relaxation after excitation. Then, the nonlinear optical absorption in BP, graphene, and MoS$_2$ was characterized by the z-scan technique, as well as measuring the differential absorptivity as a function of excitation pulse fluence [Fig. 7(a)]. BP appeared to be less nonlinear in the infrared compared to graphene, but showed much stronger saturable absorption than MoS$_2$. The results disclose that BP could be a candidate for the broadband saturable absorber in Q-switched and mode-locked lasers, as well as all-optical modulators.

Q-switched and mode-locked lasers using BP as the saturable absorber with various gain mediums and BP-integration methods have been reported.[102–112] The saturable absorption was found to be dependent on the thickness of BP.[110] According to the saturable absorption measurement, the thicker BP achieved higher modulation depth but also at the cost of a higher saturation intensity. The lower saturation energy of the thinner BP was conducive to obtaining continuous wave mode-locking operation. With a setup of BP sandwiched between the fiber end facets in series with the gain medium in the optical loop, fundamental and harmonic mode-locking in holmium-doped fiber laser was observed at a wavelength of ∼2.1 μm.[111] By increasing the pump power and adjusting the polarization controller, the tenth harmonic mode-locking could be observed to achieve a tenfold repetition rate of the fundamental mode.

For mid-infrared, Q-switched and mode-locked lasers were realized using BP as the saturable absorber and the dual-wavelength pumped Er:ZBLAN fiber as the gain medium.[112] The reflectivity dependent on the incident fluence of the BP/gold–mirror structure was measured to verify the saturable absorption in BP
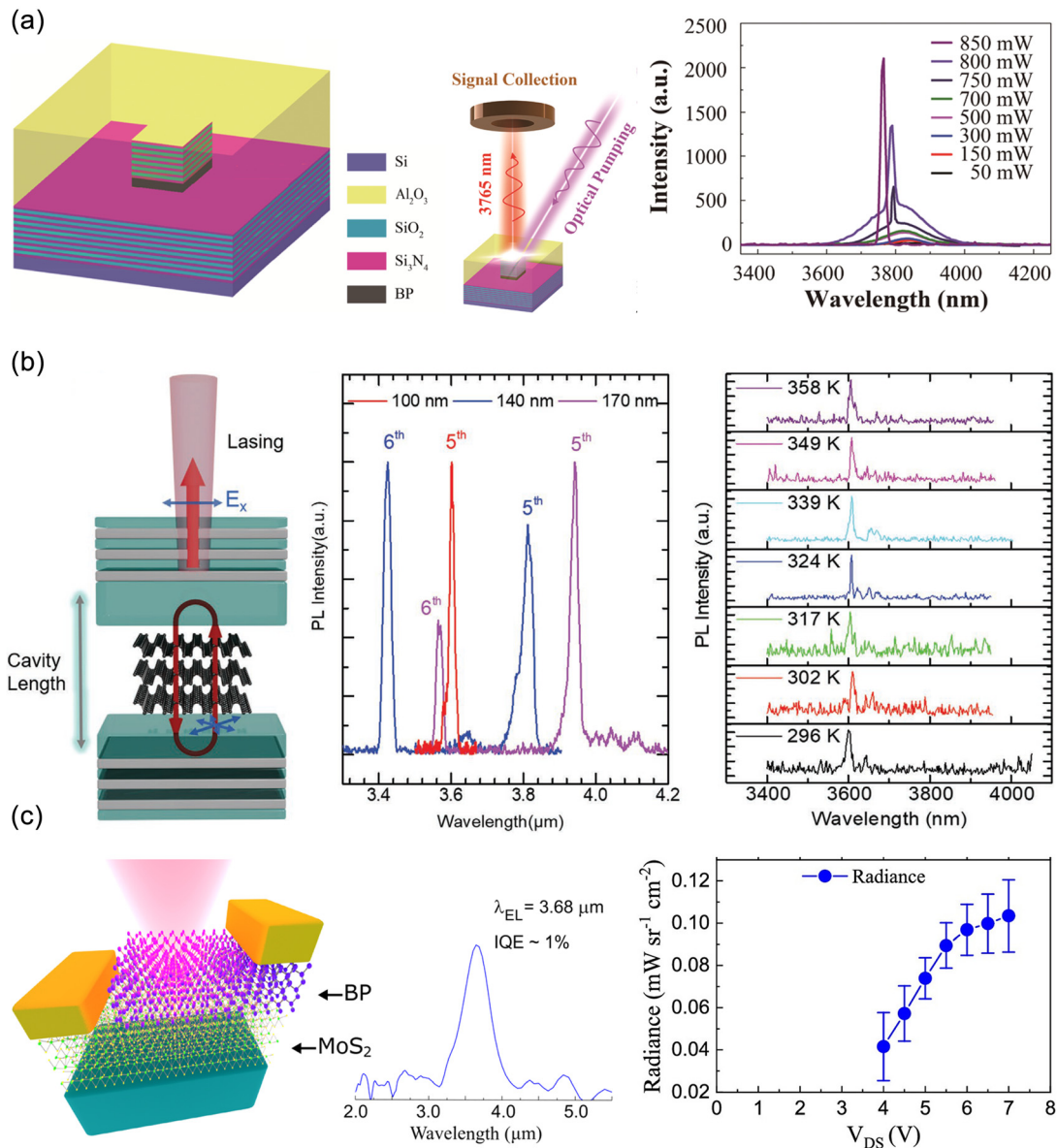
FIG. 6. Lasing and electroluminescence in BP. (a) Stimulated mid-infrared emission in BP enabled by vertical distributed Bragg reflectors (DBRs). DBRs are designed with high reflectivity at the emission wavelength of BP. Under low pumping power, the device shows spontaneous emission with a broad spectrum. Lasing occurs when the pumping power is large enough, presenting a narrow emission spectrum. Reproduced with permission from Huang *et al.*, ACS Photonics **6**(7), 1581–1586 (2019). Copyright 2019 American Chemical Society.[98] (b) Tunable lasing wavelength by BP thickness (resonant cavity length). The lasing wavelengths correspond to the DBR/BP/DBR cavity modes. Contrary to the spontaneous emission, the polarization of the lasing from the cavity is along the zigzag orientation of BP, due to a higher round trip loss for light polarized along the armchair orientation. The lasing effect is stable under room temperature and above. Reproduced with permission from Zhang *et al.*, Adv. Mater. **32**, e1808319 (2020). Copyright 2020 WILEY-VCH.[99] (c) Light emitting diode based on BP and MoS2. Electrons from the n-type MoS2 are injected into BP and recombine with holes, emitting photons with energy close to BP's bandgap. Reproduced with permission from Wang *et al.*, Nano Lett. **20**(5), 3651–3655 (2020). Copyright 2020 American Chemical Society.[100]

at 3.5 μm, indicating a modulation depth of 7.7% [Fig. 7(b)]. Two lasers at 970 and 1973 nm were used as pumps to generate an output laser from the fiber at a wavelength of 3.5 μm [Fig. 7(c)]. The operation mode of the output laser was controlled by the pump power, enabling either continuous wave, Q-switching, or continuous wave mode-locking. Under the continuous wave mode-locking operation [Figs. 7(d) and 7(e)], an output of a 40 mW average power with a repetition rate of 28.91 MHz and a signal-to-noise ratio of 54 dB were achieved, which demonstrates BP's potential for laser pulse generation in mid-infrared.
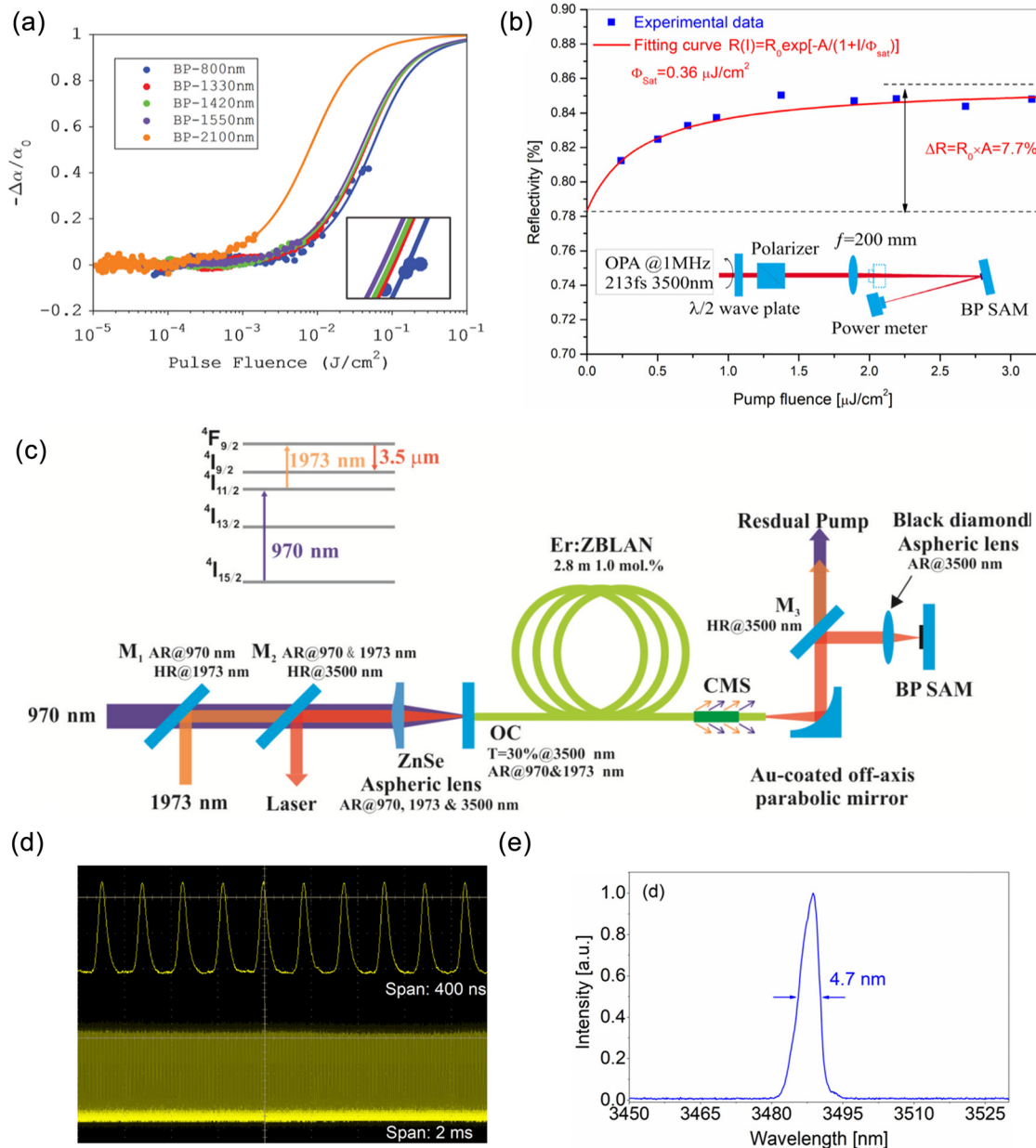
FIG. 7. Saturable absorption and laser pulse generation in BP. (a) Decreasing absorptivity under increasing excitation power for near infrared and short-wave infrared. The nonlinear absorption could be utilized for optical modulation. Reproduced with permission from Wang *et al.*, ACS Nano **10**(7), 6923–6932 (2016). Copyright 2016 American Chemical Society.[101] (b) Reflectivity modulation of 7.7% achieved by changing the pump intensity at the mid-infrared wavelength of 3.5 μm. (c) Optical setup for a 3.5 μm laser pulse generation using BP as the saturable absorber and mode-locked (d) pulse train and (e) spectrum. Two pump sources are used for the mid-infrared emission in the optical fiber. BP serves as a saturable absorber for laser pulse generation. The lasing modes are controlled by the power of the pumps. (b–e) Reproduced with permission from Qin *et al.*, Opt. Express **26**(7), 8224–8231 (2018). Copyright 2018 The Optical Society (OSA).[112]

More comprehensive summaries of the research progress on the BP saturable absorber and comparisons with other 2D materials can be found in the recent review papers.[3,19] Despite the numerous works on BP as a saturable absorber for laser pulse generation, a systematic analysis of the correlation between the laser pulse characteristic (such as repetition rate, pulse duration, and operation regime) and the parameters (such as layer number and crystal orientation) of the BP film is still lacking. Moreover, these works are all based on bulk lasers, many of which are fiber lasers of meters long. Such laser pulse generation scheme is not applicable for on-chip photonic systems. Nevertheless, based on the underlying mechanisms of these works, we could expect

that by integrating BP vertically with an optical cavity or laterally with a waveguide, it is possible to realize all-optical modulators [Fig. 8(a)], Q-switched lasers, and mode-locked lasers within chip scale.

VI. OUTLOOKS AND CHALLENGES

During the past few years, many theoretical predictions about BP's promising optical properties have been verified by experimental results, some of which have also been testified by device demonstrations. Tables I–III tabulate the performance metrics demonstrated in BP-based photodetectors, electro-optic modulation, and light emitting devices to date. By adopting different operation schemes, BP could be adapted for various optoelectronic functions, such as providing light source and converting signal between the electrical and optical ones. Through integrating these elementary functions, a comprehensive optoelectronic system could be established. Transforming the
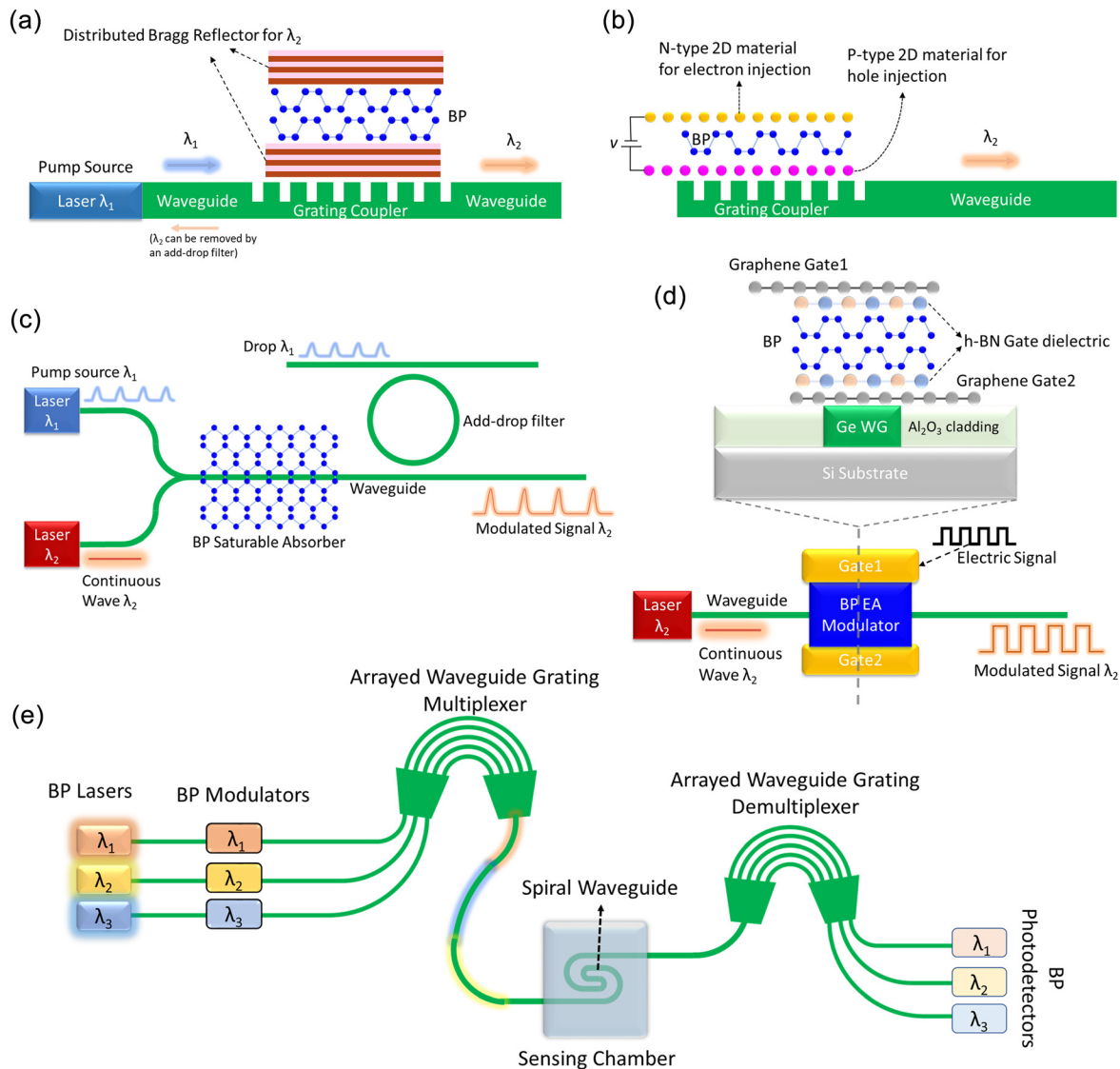
FIG. 8. Schematics of waveguide integration for photonic devices based on BP. (a) Optically pumped BP laser. Light propagation is converted between in and out of plane by grating couplers. BP sandwiched between distributed Bragg reflectors constructs a resonant cavity. (b) Electrically pumped BP light emitting diode. A p-type and an n-type 2D material are for the injection of holes and electrons, respectively. (c) BP all-optical modulator. The saturable absorption in BP is modulated by the pump source, which could be further removed from the circuit by an add-drop filter. (d) BP electro-absorption modulator. The absorption in BP is electrically controlled by the gates through the Franz–Keldysh and the Burstein–Moss effects. (e) On-chip sensing using BP photonic devices. Modulators are used to attach an on–off frequency to the light so that the signal could be differentiated from background noise. Light signals of different wavelengths are combined by the multiplexer into one channel for the interaction between light and the unknown chemical in the sensing chamber. The demultiplexer and photodetectors array serve as a spectrometer to analyze the absorption spectrum for the identification of the unknow chemical.

TABLE I. Summary of BP photodetectors.

Year	Wavelength	Device structure	BP thickness (nm)	Responsivity (A/W)	Polarization sensitivity ($R_{armchair}/R_{zigzag}$)	Detectivity (cm·Hz$^{1/2}$/W)	τ_{rise}	τ_{fall}	3-dB bandwidth	V_g (V)	V_{bias} (V)	Temperature	References
2014	400–997 nm	BP/285 nm SiO$_2$/Si	8	0.0048 at 640 nm			1 ms	4 ms		0	0.2	T_{room}	38
2014	532, 1550 nm	BP/SiO$_2$/Si	120	0.02 at 532 nm 0.005 at 1550 nm						0	−0.2	T_{room}	39
2014	633 nm	BP–MoS$_2$ heterojunction	11	0.418						40	2		55
2014	640–940 nm	Lateral BP p–n homojunction by electrostatic gating (20 nm hBN/Au)	6–7	0.00027 at 808 nm						10, −10	0	T_{room}	50
2015	400–3750 nm	Vertical BP p–n homojunction by ionic liquid gating	30–50	∼0.0003	15 at 1700 nm					2.5	0.1	T_{room}	51
2015	320–992 nm	BP/300 nm SiO$_2$/Si	4.5	9 × 10^4 at 310 nm	1.54		∼60 s at 330 nm	∼100 s at 330 nm		−80	3	T_{room}	37
2015	1550 nm	Top-gated BP/Si waveguide	11.5 100	0.135 0.657					3 GHz	−8	−0.4	T_{room}	49
2016	532 nm 1550 nm	BP–MoS$_2$ heterojunction	22	22.3 0.1534			15 μs	∼50 μs		60	3	T_{room}	56
2016	532 nm	BP–BP oxide junction	23	0.0026			∼2 s	∼5 s			0.05		59
2016	635 nm	Se doped BP	10	15.33			150 ms	300 ms		0	0.1	T_{room}	71
2016	400–900 nm	BP/90 nm SiO$_2$/Si	8	4 × 10^6 at 300 K 4 × 10^7 at 20 K						−15	−1	20–300 K	45
2016	3.39 μm	BP/90 nm SiO$_2$/Si	12	83	3–5	NEP ∼6 pW/Hz$^{1/2}$			1–3 kHz	5	0.5	T_{room}	40
2016	3.6 μm	BP/300 nm SiO$_2$/Si	10–40			10^6	65 ps	∼2 ns		0	0.2	T_{room}	42
2017	1550 nm	BP/300 nm SiO$_2$/Si	Few layer	0.006		Noise ∼10^{-10} A/Hz$^{1/2}$	<100 μs	300 μs		13.5	0.1	T_{room}	46
2017	1550 nm	BP p–n junction by Al doping	10.7	0.062 A/W 15.7 × 10^3 V/W		Estimation ∼10^{11}	3 ms	10 ms		0	0	T_{room}	52
2017	400–1550 nm	BP/WSe$_2$/300 nm SiO$_2$/Si	7	10^3–0.5	∼6	10^{14}–10^{10}	800 μs	800 μs			0.5	T_{room}	57
2017	1550 nm	Top-gated BP/Au grating/Si grating coupler-waveguide	20	6.25		I_{dark} ∼3 μA			150 MHz	−8	0.7		75
2017	2004 nm	BP/90 nm SiO$_2$/Si	23	8.5		Estimation 1.7 × 10^9			Estimation 156 kHz	12.5	−1	T_{room}	41
2017	2.5–3.7 μm	BP with interdigitated electrodes	15	0.021–0.047				∼μs	>150 kHz		0.2	T_{room}	43
2017	500–1800 nm	BP with antenna electrodes	18	0.76 at 1050 nm		NEP ∼10 pW/Hz$^{1/2}$					0.003	T_{room}	44

TABLE I. (*Continued.*)

Year	Wavelength	Device structure	BP thickness (nm)	Responsivity (A/W)	Polarization sensitivity ($R_{armchair}/R_{zigzag}$)	Detectivity (cm·Hz$^{1/2}$/W)	τ_{rise}	τ_{fall}	3-dB bandwidth	V_g (V)	V_{bias} (V)	Temperature	References
2017	1–5.5 μm	b-P b-As$_{0.91}$P$_{0.09}$/50 nm SiO$_2$/Si	36	12 at 3.5 μm	> 100	2.4 × 10^{10}	15.4 μs at 980 nm	8.6 μs at 980 nm			0.1 1	297 K	67
2017	3. 7–7.7 μm	BP with dual gates	5	0.0022 at 7.7 μm	~8 at 5 μm	NEP 672 pW/Hz$^{1/2}$			Potentially 1.3 GHz	35, −9	1.2	77 K	48
2017	2–8.2 μm	b-As$_{0.83}$P$_{0.17}$ b-As$_{0.83}$P$_{0.17}$/MoS$_2$	5–20	0.02 0.1–0.2	3.51 at 4.034 μm	2 × 10^8 5 × 10^9	0.54 ms	0.52 ms		0	0	T_{room}	58
2018	7.7 μm	hBN/b-As$_{0.83}$P$_{0.17}$/hBN/ SiO$_2$/Si	37	0.0012	1.4 at 4 μm	NEP 5 × 10^3 pW/Hz$^{1/2}$			>10 kHz	−3	1	T_{room}	68
2018	2004 nm	b-PC	7.5	2163		NEP estimation 1.3 fW/Hz$^{1/2}$				−40	0.2	T_{room}	72
2018	1550 nm	BP junction formed by a different layer number	3.3–6.1	383		Estimation 10^{10}		4 s		0	0	T_{room}	54
2018	1550 nm	BP with bowtie antenna or aperture	135	~mA/W	8.7	I_{dark} a few μA	< 90 μs	< 90 μs			0.15		65
2018	2185 nm	Chalcogenide waveguide/BP	32.4	0.04		NEP 40 pW/Hz$^{1/2}$					0.2	T_{room}	79
2018	1.3–4.3 μm	MoS$_2$/BP/Au	~150			10^{10} at 3.5 μm; 10^9 at 4 μm	3.7 μs at 2.7 μm	4 μs at 2.7 μm	100k		0	T_{room}	27
	1.4–5 μm	BP$_{armchair}$/MoS$_2$/BP$_{zigzag}$			100						±0.25		
2019	3.68–4.03 μm	BP/Si grating coupler-waveguide	23, 40	23 at 3.68 μm 2 at 4 μm (40 nm BP)	~10	NEP < 1 nW/Hz$^{1/2}$					1	T_{room}	47
2019	2 μm	BP/Si waveguide	~40	0.3067	~2.88				1.33 GHz		0.4	25–65 °C	78
2019	4 μm	BP–InSe heterojunction	10	0.0267		Dark current ~10^{-11}					−4	10 K	60
2020	400–1600 nm	BP p–n homojunction by N doping	10–20	2 at 1600 nm		NEP estimation 2.77 pW/Hz$^{1/2}$ at V_g =20 V	35 μs at 1550 nm	40 μs at 1550 nm		−40	0.1		53
2020	3.8 μm	BP/Si photonic crystal waveguide	40	11.31 at T_{room}		0.012 nW/Hz$^{1/2}$ at T_{room}			~1 kHz		0.5	23–63 °C	77

TABLE II. Summary of BP electro-optic modulation devices.

Year	Wavelength	BP thickness	Device structure	Peak modulation strength	V_g	Temperature	Ref.
2017	1.55–4.13 μm	6.5 nm	BP/285 nm SiO$_2$/Si	~2.2% at 2.38 μm	135 V	80 K	86
	1.24–4.13 μm	7 nm		2% at 2.48 μm	120 V		
	1.55–6.2 μm	14 nm		~1% at 3.54 μm	120 V		
2017	2.48–3.65 μm	9 nm	BP/450 nm SiO$_2$/Si	~1.5% at 3.26 μm	±150 V	T_{room}	87
				~2% at 2.88 μm	±50 V		
				~0.5% at 2.48 μm	±150 V		
2019	1.24–3 μm	3.5 nm	Dual gate 285 nm	30% at 2.34 μm	−80 V		28
	1.24–4.13 μm	8.5 nm	SiO$_2$/Si, 45 nm Al$_2$O$_3$/Pd	100% at 3.35 μm	−80 V		
	620–954 nm	20 nm	Dual gate 45 nm Al$_2$O$_3$/Ni $*$ 2	5%	−14 V		
2019	3.85–4.1 μm	20 nm	BP with ITO top gate/Si waveguide (interaction length: 150 μm)	~−5 dB (~68%) at 3.85 μm	−4 V	T_{room}	88

light–matter interaction from free space to guided wave regime could be a good starting point for systematic integration, as demonstrated by several experimental works on waveguide-integrated BP photodetectors,[47,49,75,76,78,79,88] as well as a BP modulator model investigated by theoretical calculations.[85] Other functions could also be incorporated into a waveguide system, as shown in Fig. 8. For example, Figs. 8(a) and 8(b) illustrate an approach to integrate waveguide with optically pumped and electrically pumped BP light emitting devices, respectively. Out-of-plane light emission from BP could be coupled into a waveguide by a grating coupler. BP as a saturable absorber could be integrated with

waveguides and an add-drop filter to realize an on-chip all-optical modulator [Fig. 8(c)], while BP sandwiched between two graphene gates placed on top of a waveguide could be a design for electro-absorption modulators [Fig. 8(d)]. In such a way, all the optoelectronic components based on BP could be further interconnected as a whole, completing an integrated photonic system. From Tables I–III, we could also notice a trend of directing the research interest to mid-infrared. The mid-infrared spectral range covers the characteristic fingerprints of many molecules. By analyzing the absorption spectrum, we could identify gases and biomolecules for applications such as environment and health

TABLE III. Summary of BP light emission devices.

Year	Emission peak wavelength	Full width at half maximum	Pump source	BP thickness	Device structure	Temperature	Ref.
2014	961 nm	~100 nm	532 nm	2 layers	BP/275 nm SiO$_2$/Si	T_{room}	89
	1268 nm			3 layers			
	1413 nm			4 layers			
	1558 nm			5 layers			
2015	~550 nm	~170 nm	330–380 nm	Few-layer phosphorene oxide	Phosphorene oxide/SiO$_2$/Si		90
	~560 nm	~100 nm	460–490 nm				
	~625 nm	~90 nm	510–550 nm				
	~650 nm	~80 nm	550–580 nm				
2017	~729 nm	~36 nm	532 nm	Monolayer	BP/300 nm SiO$_2$/Si	77 K	91
	~1127 nm	~68 nm		2 layers			
	~1282 nm	~80 nm		3 layers			
2019	4 μm	~417 nm	640 nm	46 nm	hBN/BP/300 nm SiO$_2$/Si	80 K	96
	3.73 μm	~511 nm				300 K	
2019	3836 nm	190 nm	50 mW 740 nm	1 μm	DBR/Lamellar BP/DBR/Si DBR: distributed Bragg reflector (SiO$_2$/Si$_3$N$_4$)	T_{room}	98
	3765 nm	<9 nm	850 mW				
2020	3.68 μm	~750 nm	808 nm	70 nm	Au–BP–10 nm MoS$_2$–Au/90 nm SiO$_2$/Si Light emitting diode	T_{room}	100
		~425 nm	$V_{ds} = 7$ V				
2020	3.7 μm $V_g = 0$ V	~330 nm	640 nm	10.5 nm	Graphene/9 nm hBN/BP/22 nm hBN/ SiO$_2$/Si	83 K	97
	7.7 μm $V_g = 40$ V	~840 nm					
2020	3425–4068 nm	7 nm	1064 nm 1520 nm	38–220 nm	DBR/BP/DBR DBR: Si/SiO$_2$	Up to 360 K	99

monitoring. Figure 8(e) shows a schematic of a BP photonic circuit for on-chip sensing applications. The arrayed waveguide grating multiplexer combines light sources of varying wavelengths into one waveguide in the sensing chamber, where the interaction between light and the unknown chemical takes place. The demultiplexer and photodetectors serve as a spectrometer to analyze the absorption spectrum of the chemical. Modulators could attach an on–off frequency to the light so that weak signals could be extracted from a noisy background. The active components (lasers, modulators, and photodetectors) in the circuit could be realized using an all-BP platform, as illustrated in Figs. 2 and 8(a)–8(d), while we could leverage on the well-developed Si and Ge technologies for the passive components (waveguides, couplers, and resonators).

Although the preliminary investigations have revealed BP's attractive potential for providing a solution to integrated photonic systems, some challenges remain to be addressed. The ambient degradation of BP is no longer a limiting factor as it could be effectively prevented by a passivation layer such as hexagonal boron nitride (hBN) or alumina.[113,114] Meanwhile, the large scale growth of high-quality BP could be a bottleneck for developing BP-based technology. So far, there are some works of synthesizing thin film BP on Si, sapphire, and flexible substrates.[115–118] However, more efforts are needed to improve the crystallinity, the scale of continuous growth, and the controllability of BP thin films. Control over the crystal orientation, doping condition, defect level, and thickness of the BP thin films is of vital importance to its optoelectronic performance, such as responsivity, speed, noise level, modulation efficiency, and light emission efficiency. Apart from the inherent material properties, the device configuration also plays a critical role in determining the eventual performance of the device. For example, the material selection and layout of the electrodes may affect the light distribution, carrier collection, and injection. In addition, the optical environment (such as the substrate and cladding) around BP could impact the external efficiency of light detection and emission. To achieve highly efficient light emitting devices based on BP, assistive optical structures may be needed to extract light emission from BP to the desired spatial region. Applications, such as data communication and LiDAR, require high speed operation. Besides optimizing the device geometry to improve the speed performance, stacking BP with other 2D materials to form heterostructures is another approach to control carrier dynamics, so as to boost speed, suppress dark current, and enhance the efficiency of electron–photon conversion. In addition, patterning the thin film BP into a periodic structure could be explored in order to induce optical resonance,[34,119–121] which may enable better wavelength and polarization selectivity, as well as more effective light modulation. In order to bring out the best in BP, more endeavors need to be devoted to device design (both electrical and optical) and optimization. With continued research efforts focused on BP, we could envisage a bright future for BP photonics, where the expectations and proof-of-concepts could be turned into practical applications.

ACKNOWLEDGMENTS

DATA AVAILABILITY

Data sharing is not applicable to this article as no new data were created or analyzed in this study.

REFERENCES

[1]F. Xia, H. Wang, J. C. M. Hwang, A. H. C. Neto, and L. Yang, Nat. Rev. Phys. **1**(5), 306–317 (2019).
[2]B. Deng, R. Frisenda, C. Li, X. Chen, A. Castellanos-Gomez, and F. Xia, Adv. Opt. Mater. **6**(19), 1800365 (2018).
[3]Y. Fang, Y. Ge, C. Wang, and H. Zhang, Laser Photonics Rev. **14**(1), 1900098 (2020).
[4]G. Fiori, F. Bonaccorso, G. Iannaccone, T. Palacios, D. Neumaier, A. Seabaugh, S. K. Banerjee, and L. Colombo, Nat. Nanotechnol. **9**(10), 768–779 (2014).
[5]F. Xia, H. Wang, D. Xiao, M. Dubey, and A. Ramasubramaniam, Nat. Photonics **8**(12), 899–907 (2014).
[6]X. Ling, H. Wang, S. Huang, F. Xia, and M. S. Dresselhaus, Proc. Natl. Acad. Sci. U. S. A. **112**(15), 4523–4530 (2015).
[7]H. Asahina and A. Morita, J. Phys. C: Solid State Phys. **17**(11), 1839–1852 (1984).
[8]J. Qiao, X. Kong, Z. X. Hu, F. Yang, and W. Ji, Nat. Commun. **5**, 4475 (2014).
[9]L. Li, Y. Yu, G. J. Ye, Q. Ge, X. Ou, H. Wu, D. Feng, X. H. Chen, and Y. Zhang, Nat. Nanotechnol. **9**(5), 372–377 (2014).
[10]L. Li, F. Yang, G. J. Ye, Z. Zhang, Z. Zhu, W. Lou, X. Zhou, L. Li, K. Watanabe, T. Taniguchi, K. Chang, Y. Wang, X. H. Chen, and Y. Zhang, Nat. Nanotechnol. **11**(7), 593–597 (2016).
[11]V. Tran, R. Soklaski, Y. Liang, and L. Yang, Phys. Rev. B **89**(23), 235319 (2014).
[12]R. Soref, Nat. Photonics **4**(8), 495–497 (2010).
[13]A. Castellanos-Gomez, J. Phys. Chem. Lett. **6**(21), 4280–4291 (2015).
[14]Y. Li, S. Yang, and J. Li, J. Phys. Chem. C **118**(41), 23970–23976 (2014).
[15]B. Deng, V. Tran, Y. Xie, H. Jiang, C. Li, Q. Guo, X. Wang, H. Tian, S. J. Koester, H. Wang, J. J. Cha, Q. Xia, L. Yang, and F. Xia, Nat. Commun. **8**, 14474 (2017).
[16]K. Dolui and S. Y. Quek, Sci. Rep. **5**, 11699 (2015).
[17]Y. Liu, Z. Qiu, A. Carvalho, Y. Bao, H. Xu, S. J. Tan, W. Liu, A. H. Castro Neto, K. P. Loh, and J. Lu, Nano Lett. **17**(3), 1970–1977 (2017).
[18]Z. Sun, A. Martinez, and F. Wang, Nat. Photonics **10**(4), 227–238 (2016).
[19]M. Zhang, Q. Wu, F. Zhang, L. Chen, X. Jin, Y. Hu, Z. Zheng, and H. Zhang, Adv. Opt. Mater. **7**(1), 1800224 (2019).
[20]T. Low, A. S. Rodin, A. Carvalho, Y. Jiang, H. Wang, F. Xia, and A. H. Castro Neto, Phys. Rev. B **90**(7), 075434 (2014).
[21]X. Ling, S. Huang, E. H. Hasdeo, L. Liang, W. M. Parkin, Y. Tatsumi, A. R. Nugraha, A. A. Puretzky, P. M. Das, B. G. Sumpter, D. B. Geohegan, J. Kong, R. Saito, M. Drndic, V. Meunier, and M. S. Dresselhaus, Nano Lett. **16**(4), 2260–2267 (2016).
[22]H. B. Ribeiro, M. A. Pimenta, C. J. de Matos, R. L. Moreira, A. S. Rodin, J. D. Zapata, E. A. de Souza, and A. H. Castro Neto, ACS Nano **9**(4), 4270–4276 (2015).
[23]G. Zhang, S. Huang, A. Chaves, C. Song, V. O. Ozcelik, T. Low, and H. Yan, Nat. Commun. **8**, 14071 (2017).
[24]X. Wang, A. M. Jones, K. L. Seyler, V. Tran, Y. Jia, H. Zhao, H. Wang, L. Yang, X. Xu, and F. Xia, Nat. Nanotechnol. **10**(6), 517–521 (2015).
[25]J. Yang, R. Xu, J. Pei, Y. W. Myint, F. Wang, Z. Wang, S. Zhang, Z. Yu, and Y. Lu, e Light: Sci. Appl. **4**(7), e312–e312 (2015).
[26]A. Morita, Appl. Phys. A: Solids Surf. **39**(4), 227–242 (1986).
[27]J. Bullock, M. Amani, J. Cho, Y.-Z. Chen, G. H. Ahn, V. Adinolfi, V. R. Shrestha, Y. Gao, K. B. Crozier, Y.-L. Chueh, and A. Javey, Nat. Photonics **12**(10), 601–607 (2018).
[28]M. C. Sherrott, W. S. Whitney, D. Jariwala, S. Biswas, C. M. Went, J. Wong, G. R. Rossman, and H. A. Atwater, Nano Lett. **19**(1), 269–276 (2019).
[29]M. Razeghi and B. M. Nguyen, Rep. Prog. Phys. **77**(8), 082401 (2014).
[30]P. Martyniuk, J. Antoszewski, M. Martyniuk, L. Faraone, and A. Rogalski, Appl. Phys. Rev. **1**(4), 041102 (2014).
[31]Z. Fang and C. Z. Zhao, ISRN Opt. **2012**, 1–27.

[32]D. Thomson, A. Zilkie, J. E. Bowers, T. Komljenovic, G. T. Reed, L. Vivien, D. Marris-Morini, E. Cassan, L. Virot, J.-M. Fédéli, J.-M. Hartmann, J. H. Schmid, D.-X. Xu, F. Boeuf, P. O'Brien, G. Z. Mashanovich, and M. Nedeljkovic, J. Opt. **18**(7), 073003 (2016).

[33]R. Soref, Proc. SPIE **8629**, 862902–862901 (2013).

[34]D. Rodrigo, O. Limaj, D. Janner, D. Etezadi, F. J. Garcia de Abajo, V. Pruneri, and H. Altug, Science **349**(6244), 165–168 (2015).

[35]D. Ouzounov and F. Freund, Adv. Space Res. **33**(3), 268–273 (2004).

[36]D. Akinwande, C. Huyghebaert, C. H. Wang, M. I. Serna, S. Goossens, L. J. Li, H. P. Wong, and F. H. L. Koppens, Nature **573**(7775), 507–518 (2019).

[37]J. Wu, G. K. Koon, D. Xiang, C. Han, C. T. Toh, E. S. Kulkarni, I. Verzhbitskiy, A. Carvalho, A. S. Rodin, S. P. Koenig, G. Eda, W. Chen, A. H. Neto, and B. Ozyilmaz, ACS Nano **9**(8), 8070–8077 (2015).

[38]M. Buscema, D. J. Groenendijk, S. I. Blanter, G. A. Steele, H. S. van der Zant, and A. Castellanos-Gomez, Nano Lett. **14**(6), 3347–3352 (2014).

[39]M. Engel, M. Steiner, and P. Avouris, Nano Lett. **14**(11), 6414–6417 (2014).

[40]Q. Guo, A. Pospischil, M. Bhuiyan, H. Jiang, H. Tian, D. Farmer, B. Deng, C. Li, S. J. Han, H. Wang, Q. Xia, T. P. Ma, T. Mueller, and F. Xia, Nano Lett. **16**(7), 4648–4655 (2016).

[41]L. Huang, W. C. Tan, L. Wang, B. Dong, C. Lee, and K.-W. Ang, ACS Appl. Mater. Interfaces **9**(41), 36130–36136 (2017).

[42]R. J. Suess, E. Leong, J. L. Garrett, T. Zhou, R. Salem, J. N. Munday, T. E. Murphy, and M. Mittendorff, 2D Mater. **3**(4), 041006 (2016).

[43]M. Xu, Y. Gu, R. Peng, N. Youngblood, and M. Li, Appl. Phys. B **123**(4), 130 (2017).

[44]L. Wang, C. Liu, X. Chen, J. Zhou, W. Hu, X. Wang, J. Li, W. Tang, A. Yu, S.-W. Wang, and W. Lu, Adv. Funct. Mater. **27**(7), 1604414 (2017).

[45]M. Huang, M. Wang, C. Chen, Z. Ma, X. Li, J. Han, and Y. Wu, Adv. Mater. **28**(18), 3481–3485 (2016).

[46]J. Na, K. Park, J. T. Kim, W. K. Choi, and Y. W. Song, Nanotechnology **28**(8), 085201 (2017).

[47]L. Huang, B. Dong, X. Guo, Y. Chang, N. Chen, X. Huang, W. Liao, C. Zhu, H. Wang, C. Lee, and K.-W. Ang, ACS Nano **13**(1), 913–921 (2019).

[48]X. Chen, X. Lu, B. Deng, O. Sinai, Y. Shao, C. Li, S. Yuan, V. Tran, K. Watanabe, T. Taniguchi, D. Naveh, L. Yang, and F. Xia, Nat. Commun. **8**(1), 1672 (2017).

[49]N. Youngblood, C. Chen, S. J. Koester, and M. Li, Nat. Photonics **9**(4), 247–252 (2015).

[50]M. Buscema, D. J. Groenendijk, G. A. Steele, H. S. van der Zant, and A. Castellanos-Gomez, Nat. Commun. **5**, 4651 (2014).

[51]H. Yuan, X. Liu, F. Afshinmanesh, W. Li, G. Xu, J. Sun, B. Lian, A. G. Curto, G. Ye, Y. Hikita, Z. Shen, S. C. Zhang, X. Chen, M. Brongersma, H. Y. Hwang, and Y. Cui, Nat. Nanotechnol. **10**(8), 707–713 (2015).

[52]Y. Liu, Y. Cai, G. Zhang, Y.-W. Zhang, and K.-W. Ang, Adv. Funct. Mater. **27**(7), 1604638 (2017).

[53]Y. Xu, C. Liu, C. Guo, Q. Yu, W. Guo, W. Lu, X. Chen, L. Wang, and K. Zhang, Nano Energy **70**, 104518 (2020).

[54]L. Wang, L. Huang, W. C. Tan, X. Feng, L. Chen, and K.-W. Ang, Nanoscale **10**(29), 14359–14367 (2018).

[55]Y. Deng, Z. Luo, N. J. Conrad, H. Liu, Y. Gong, S. Najmaei, P. M. Ajayan, J. Lou, X. Xu, and P. D. Ye, ACS Nano **8**(8), 8292–8299 (2014).

[56]L. Ye, H. Li, Z. Chen, and J. Xu, ACS Photonics **3**(4), 692–699 (2016).

[57]L. Ye, P. Wang, W. Luo, F. Gong, L. Liao, T. Liu, L. Tong, J. Zang, J. Xu, and W. Hu, Nano Energy **37**, 53–60 (2017).

[58]M. Long, A. Gao, P. Wang, H. Xia, C. Ott, C. Pan, Y. Fu, E. Liu, X. Chen, W. Lu, T. Nilges, J. Xu, X. Wang, W. Hu, and F. Miao, Sci. Adv. **3**(6), e1700589 (2017).

[59]J. Lu, A. Carvalho, J. Wu, H. Liu, E. S. Tok, A. H. Neto, B. Ozyilmaz, and C. H. Sow, Adv. Mater. **28**(21), 4090–4096 (2016).

[60]A. Gao, J. Lai, Y. Wang, Z. Zhu, J. Zeng, G. Yu, N. Wang, W. Chen, T. Cao, W. Hu, D. Sun, X. Chen, F. Miao, Y. Shi, and X. Wang, Nat. Nanotechnol. **14**(3), 217–222 (2019).

[61]F. Xia, H. Wang, and Y. Jia, Nat. Commun. **5**, 4458 (2014).

[62]M. Garcia, T. Davis, S. Blair, N. Cui, and V. Gruev, Optica **5**(10), 1240–1246 (2018).

[63]R. D. Tooley, Proc. SPIE **1166**, 52–58 (1990).

[64]S. A. Empedocles, R. Neuhauser, and M. G. Bawendi, Nature **399**(6732), 126–130 (1999).

[65]P. K. Venuthurumilli, P. D. Ye, and X. Xu, ACS Nano **12**(5), 4861–4867 (2018).

[66]B. Liu, M. Kopf, A. N. Abbas, X. Wang, Q. Guo, Y. Jia, F. Xia, R. Weihrich, F. Bachhuber, F. Pielnhofer, H. Wang, R. Dhall, S. B. Cronin, M. Ge, X. Fang, T. Nilges, and C. Zhou, Adv. Mater. **27**(30), 4423–4429 (2015).

[67]M. Amani, E. Regan, J. Bullock, G. H. Ahn, and A. Javey, ACS Nano **11**(11), 11724–11731 (2017).

[68]S. Yuan, C. Shen, B. Deng, X. Chen, Q. Guo, Y. Ma, A. Abbas, B. Liu, R. Haiges, C. Ott, T. Nilges, K. Watanabe, T. Taniguchi, O. Sinai, D. Naveh, C. Zhou, and F. Xia, Nano Lett. **18**(5), 3172–3179 (2018).

[69]D. Caffey, M. B. Radunsky, V. Cook, M. Weida, P. R. Buerki, S. Crivello, and T. Day, "Recent results from broadly tunable external cavity quantum cascade lasers," in Proc. SPIE 7953, Novel In-Plane Semiconductor Lasers X, 79531K (SPIE, 2011), p. 79531K.

[70]J. Kim, S. S. Baik, S. H. Ryu, Y. Sohn, S. Park, B. G. Park, J. Denlinger, Y. Yi, H. J. Choi, and K. S. Kim, Science **349**(6249), 723–726 (2015).

[71]Y. Xu, J. Yuan, L. Fei, X. Wang, Q. Bao, Y. Wang, K. Zhang, and Y. Zhang, Small **12**(36), 5000–5007 (2016).

[72]W. C. Tan, L. Huang, R. J. Ng, L. Wang, D. M. N. Hasan, T. J. Duffin, K. S. Kumar, C. A. Nijhuis, C. Lee, and K.-W. Ang, Adv. Mater. **30**(6), 1705039 (2018).

[73]W. C. Tan, L. Huang, R. J. Ng, L. Wang, and K.-W. Ang, in 2017 IEEE International Electron Devices Meeting (IEDM), San Francisco, USA 2017, pp. 8.4.1–8.4.4.

[74]T. Yin, R. Cohen, M. M. Morse, G. Sarid, Y. Chetrit, D. Rubin, and M. J. Paniccia, Opt. Express **15**(21), 13965–13971 (2007).

[75]C. Chen, N. Youngblood, R. Peng, D. Yoo, D. A. Mohr, T. W. Johnson, S. H. Oh, and M. Li, Nano Lett. **17**(2), 985–991 (2017).

[76]T. Wang, S. Hu, B. Chamlagain, T. Hong, Z. Zhou, S. M. Weiss, and Y. Q. Xu, Adv. Mater. **28**(33), 7162–7166 (2016).

[77]Y. Ma, B. Dong, J. Wei, Y. Chang, L. Huang, K.-W. Ang, and C. Lee, Adv. Optic. Mater. **8**, 2000337 (2020).

[78]Y. Yin, R. Cao, J. Guo, C. Liu, J. Li, X. Feng, H. Wang, W. Du, A. Qadir, H. Zhang, Y. Ma, S. Gao, Y. Xu, Y. Shi, L. Tong, and D. Dai, Laser Photonics Rev. **13**, 1900032 (2019).

[79]S. Deckoff-Jones, H. Lin, D. Kita, H. Zheng, D. Li, W. Zhang, and J. Hu, J. Opt. **20**(4), 044004 (2018).

[80]L. Huang, B. Dong, X. Guo, Y. Chang, N. Chen, X. Huang, H. Wang, C. Lee, and K.-W. Ang, in 2018 IEEE Symposium on VLSI Technology, Honolulu, USA, 2018, pp. 161–162.

[81]G. T. Reed, G. Mashanovich, F. Y. Gardes, and D. J. Thomson, Nat. Photonics **4**(8), 518–526 (2010).

[82]G. Marriott, S. Mao, T. Sakata, J. Ran, D. K. Jackson, C. Petchprayoon, T. J. Gomez, E. Warp, O. Tulyathan, H. L. Aaron, E. Y. Isacoff, and Y. Yan, Proc. Natl. Acad. Sci. U. S. A. **105**(46), 17789–17794 (2008).

[83]M. J. R. Heck, Nanophotonics **6**(1), 93–107 (2017).

[84]H. Guo, N. Lu, J. Dai, X. Wu, and X. C. Zeng, J. Phys. Chem. C **118**(25), 14051–14059 (2014).

[85]C. Lin, R. Grassi, T. Low, and A. S. Helmy, Nano Lett. **16**(3), 1683–1689 (2016).

[86]W. S. Whitney, M. C. Sherrott, D. Jariwala, W. H. Lin, H. A. Bechtel, G. R. Rossman, and H. A. Atwater, Nano Lett. **17**(1), 78–84 (2017).

[87]R. Peng, K. Khaliji, N. Youngblood, R. Grassi, T. Low, and M. Li, Nano Lett. **17**(10), 6315–6320 (2017).

[88]L. Huang, B. Dong, Y. Ma, C. Lee, and K.-W. Ang, in 2019 IEEE International Electron Devices Meeting (IEDM), San Francisco, USA, 2019, pp. 33.36.31–33.36.34.

[89]S. Zhang, J. Yang, R. Xu, F. Wang, W. Li, M. Ghufran, Y. W. Zhang, Z. Yu, G. Zhang, Q. Qin, and Y. Lu, ACS Nano **8**(9), 9590–9596 (2014).

[90]J. Lu, J. Wu, A. Carvalho, A. Ziletti, H. Liu, J. Tan, Y. Chen, A. H. Castro Neto, B. Ozyilmaz, and C. H. Sow, ACS Nano **9**(10), 10411–10421 (2015).

[91]L. Li, J. Kim, C. Jin, G. J. Ye, D. Y. Qiu, F. H. da Jornada, Z. Shi, L. Chen, Z. Zhang, F. Yang, K. Watanabe, T. Taniguchi, W. Ren, S. G. Louie, X. H. Chen, Y. Zhang, and F. Wang, Nat. Nanotechnol. **12**(1), 21–25 (2017).

[92]G. Zhang, A. Chaves, S. Huang, F. Wang, Q. Xing, T. Low, and H. Yan, Sci. Adv. **4**(3), eaap9977 (2018).

[93] A. Castellanos-Gomez, L. Vicarelli, E. Prada, J. O. Island, K. L. Narasimha-Acharya, S. I. Blanter, D. J. Groenendijk, M. Buscema, G. A. Steele, J. V. Alvarez, H. W. Zandbergen, J. J. Palacios, and H. S. J. van der Zant, 2D Mater. **1**(2), 025001 (2014).

[94] A. Chaves, T. Low, P. Avouris, D. Çakır, and F. M. Peeters, Phys. Rev. B **91**(15), 155311 (2015).

[95] R. Xu, J. Yang, Y. W. Myint, J. Pei, H. Yan, F. Wang, and Y. Lu, Adv. Mater. **28**(18), 3493–3498 (2016).

[96] C. Chen, F. Chen, X. Chen, B. Deng, B. Eng, D. Jung, Q. Guo, S. Yuan, K. Watanabe, T. Taniguchi, M. L. Lee, and F. Xia, Nano Lett. **19**(3), 1488–1493 (2019).

[97] C. Chen, X. Lu, B. Deng, X. Chen, Q. Guo, C. Li, C. Ma, S. Yuan, E. Sung, K. Watanabe, T. Taniguchi, L. Yang, and F. Xia, Sci. Adv. **6**(7), eaay6134 (2020).

[98] Y. Huang, J. Ning, H. Chen, Y. Xu, X. Wang, X. Ge, C. Jiang, X. Zhang, J. Zhang, Y. Peng, Z. Huang, Y. Ning, K. Zhang, and Z. Zhang, ACS Photonics **6**(7), 1581–1586 (2019).

[99] Y. Zhang, S. Wang, S. Chen, Q. Zhang, X. Wang, X. Zhu, X. Zhang, X. Xu, T. Yang, M. He, X. Yang, Z. Li, X. Chen, M. Wu, Y. Lu, R. Ma, W. Lu, and A. Pan, Adv. Mater. **32**, e1808319 (2020).

[100] J. Wang, A. Rousseau, M. Yang, T. Low, S. Francoeur, and S. Kena-Cohen, Nano Lett. **20**(5), 3651–3655 (2020).

[101] K. Wang, B. M. Szydlowska, G. Wang, X. Zhang, J. J. Wang, J. J. Magan, L. Zhang, J. N. Coleman, J. Wang, and W. J. Blau, ACS Nano **10**(7), 6923–6932 (2016).

[102] L. Kong, Z. Qin, G. Xie, Z. Guo, H. Zhang, P. Yuan, and L. Qian, Laser Phys. Lett. **13**(4), 045801 (2016).

[103] Z. C. Luo, M. Liu, Z. N. Guo, X. F. Jiang, A. P. Luo, C. J. Zhao, X. F. Yu, W. C. Xu, and H. Zhang, Opt. Express **23**(15), 20030–20039 (2015).

[104] Z. Qin, G. Xie, H. Zhang, C. Zhao, P. Yuan, S. Wen, and L. Qian, Opt. Express **23**(19), 24713–24718 (2015).

[105] Z. Qin, G. Xie, C. Zhao, S. Wen, P. Yuan, and L. Qian, Opt. Lett. **41**(1), 56–59 (2016).

[106] J. Sotor, G. Sobon, M. Kowalczyk, W. Macherzynski, P. Paletko, and K. M. Abramski, Opt. Lett. **40**(16), 3885–3888 (2015).

[107] Y. Xie, L. Kong, Z. Qin, G. Xie, and J. Zhang, Opt. Eng. **55**(8), 081307 (2016).

[108] H. Yu, X. Zheng, K. Yin, X. a Cheng, and T. Jiang, Opt. Mater. Express **6**(2), 603 (2016).

[109] R. Zhang, Y. Zhang, H. Yu, H. Zhang, R. Yang, B. Yang, Z. Liu, and J. Wang, Adv. Opt. Mater. **3**(12), 1787–1792 (2015).

[110] Y. Chen, G. Jiang, S. Chen, Z. Guo, X. Yu, C. Zhao, H. Zhang, Q. Bao, S. Wen, D. Tang, and D. Fan, Opt. Express **23**(10), 12823–12833 (2015).

[111] M. Pawliszewska, Y. Ge, Z. Li, H. Zhang, and J. Sotor, Opt. Express **25**(15), 16916–16921 (2017).

[112] Z. Qin, T. Hai, G. Xie, J. Ma, P. Yuan, L. Qian, L. Li, L. Zhao, and D. Shen, Opt. Express **26**(7), 8224–8231 (2018).

[113] R. A. Doganov, E. C. O'Farrell, S. P. Koenig, Y. Yeo, A. Ziletti, A. Carvalho, D. K. Campbell, D. F. Coker, K. Watanabe, T. Taniguchi, A. H. Castro Neto, and B. Ozyilmaz, Nat. Commun. **6**, 6647 (2015).

[114] J. D. Wood, S. A. Wells, D. Jariwala, K. S. Chen, E. Cho, V. K. Sangwan, X. Liu, L. J. Lauhon, T. J. Marks, and M. C. Hersam, Nano Lett. **14**(12), 6964–6970 (2014).

[115] C. Li, Y. Wu, B. Deng, Y. Xie, Q. Guo, S. Yuan, X. Chen, M. Bhuiyan, Z. Wu, K. Watanabe, T. Taniguchi, H. Wang, J. J. Cha, M. Snure, Y. Fei, and F. Xia, Adv. Mater. **30**(6), 1703748 (2018).

[116] X. Li, B. Deng, X. Wang, S. Chen, M. Vaisman, S-i Karato, G. Pan, M. Larry Lee, J. Cha, H. Wang, and F. Xia, 2D Mater. **2**(3), 031002 (2015).

[117] J. B. Smith, D. Hagaman, and H. F. Ji, Nanotechnology **27**(21), 215602 (2016).

[118] Y. Xu, X. Shi, Y. Zhang, H. Zhang, Q. Zhang, Z. Huang, X. Xu, J. Guo, H. Zhang, L. Sun, Z. Zeng, A. Pan, and K. Zhang, Nat. Commun. **11**(1), 1330 (2020).

[119] V. W. Brar, M. S. Jang, M. Sherrott, S. Kim, J. J. Lopez, L. B. Kim, M. Choi, and H. Atwater, Nano Lett. **14**(7), 3876–3880 (2014).

[120] L. Ju, B. Geng, J. Horng, C. Girit, M. Martin, Z. Hao, H. A. Bechtel, X. Liang, A. Zettl, Y. R. Shen, and F. Wang, Nat. Nanotechnol. **6**(10), 630–634 (2011).

[121] H. Yan, X. Li, B. Chandra, G. Tulevski, Y. Wu, M. Freitag, W. Zhu, P. Avouris, and F. Xia, Nat. Nanotechnol. **7**(5), 330–334 (2012).